

# Optimal Thinning of MCMC Output

Marina Riabiz<sup>1,2</sup>, Wilson Chen<sup>3</sup>, Jon Cockayne<sup>2</sup>, Paweł Swietach<sup>4</sup>,  
 Steve Niederer<sup>1</sup>, Lester Mackey<sup>5</sup>, Chris Oates<sup>6,2</sup>

<sup>1</sup>King’s College London, UK

<sup>2</sup>Alan Turing Institute, UK

<sup>3</sup>University of Sydney, Australia

<sup>4</sup>Oxford University, UK

<sup>5</sup>Microsoft Research, US

<sup>6</sup>Newcastle University, UK

May 17, 2022

## Abstract

The use of heuristics to assess the convergence and compress the output of Markov chain Monte Carlo can be sub-optimal in terms of the empirical approximations that are produced. Typically a number of the initial states are attributed to “burn in” and removed, whilst the chain can be “thinned” if compression is also required. In this paper we consider the problem of selecting a subset of states, of fixed cardinality, such that the approximation provided by their empirical distribution is close to optimal. A novel method is proposed, based on greedy minimisation of a kernel Stein discrepancy, that is suitable for problems where heavy compression is required. Theoretical results guarantee consistency of the method and its effectiveness is demonstrated in the challenging context of parameter inference for ordinary differential equations. Software is available in the **Stein Thinning** package in both Python and MATLAB, and example code is included.

## 1 Introduction

The most popular computational tool for Bayesian inference outside the setting of conjugate exponential families is Markov chain Monte Carlo (MCMC). Introduced to statistics from the physics literature in Hastings (1970); Geman and Geman (1984); Tanner and Wong (1987); Gelfand and Smith (1990), an enormous amount of research effort has since been expended in the advancement of MCMC methodology. Indeed, such is the breadth of this topic that we do not attempt to provide a survey here, but instead refer the reader to Robert and Casella (2013); Green et al. (2015) and the references therein to more advanced material.

This paper is motivated by the fact that assessing convergence and post-processing the output of MCMC methods is a relevant, but still unsolved, topic in computational statistics, that can strongly affect the estimates that are produced. Often we are interested in a distribution  $P$ , supported, say, on  $\mathbb{R}^d$ , and we wish to obtain an approximation of the integral

$$I_P(f) := \int_{\mathbb{R}^d} f(x) dP(x), \quad (1)$$

for a given  $P$ -integrable function  $f : \mathbb{R}^d \rightarrow \mathbb{R}^l$ . In many cases, (1) cannot be computed analytically, nor it is possible to obtain independent samples from  $P$  for direct Monte Carlo integration. However, it is instead often possible to simulate a finite portion of a Markov chain  $(X_i)_{i \in \mathbb{N}}$ , whose invariant distribution is  $P$ . Under standard conditions (e.g. that the Markov chain is positive Harris; see Theorem 17.0.1 of Meyn and Tweedie, 2012) the law of large numbers can be shown to hold, meaning that almost surely

$$\frac{1}{n} \sum_{i=1}^n f(X_i) \rightarrow I_P(f) \quad (2)$$

as  $n \rightarrow \infty$ . Our discussion supposes that a practitioner is prepared to simulate a Markov chain up to a maximum number of iterations,  $n$ , and that simulating further iterations is not practical; a scenario that is often encountered (e.g. see Section 4.4). The approximation quality of the estimator in (2) then depends on which states  $X_i$  were visited on the sample path that was simulated. In practice, it is common (and indeed recommended) to replace (2) with an alternative estimator

$$\frac{1}{m} \sum_{j=1}^m f(X_{\pi(j)}) \quad (3)$$

that is based on a subset of the total MCMC output. The  $m$  indices  $\pi(j) \in \{1, \dots, n\}$ ,  $j = 1, \dots, m$ , indicate which states are retained and the identification of a suitable index set,  $\pi$ , is informed by the following considerations:

**Removal of Initial Bias:** The distribution of the initial state,  $X_0$ , of the Markov chain will not typically equal  $P$ , otherwise independent sampling from  $P$  should be preferred to MCMC. Therefore the distribution of several of the early states of the chain may be quite different to  $P$ . To mitigate this, it is desirable to estimate a period  $b \in \mathbb{N}$ , after which each of the states  $(X_i)_{i>b}$ , can be reasonably considered to be distributed according to  $P$ . The index set  $\pi$  would then be selected such that the first states  $(X_i)_{i=1}^b$ , often referred to as a “burn-in” period, are not included.

Rigorous approaches for selecting  $b$  were proposed by authors including Meyn and Tweedie (1994); Rosenthal (1995); Roberts and Tweedie (1999); see also Jones and Hobert (2001). Unfortunately, these often involve conditions that are difficult to establish in practical settings, or, when they hold, they provide loose bounds, implying to an unreasonably long

burn-in period. The difficulties of selecting  $b$  have led to the use of heuristics for convergence diagnosis (Cowles and Carlin, 1996). These are typically based on the empirical distribution of simple moment, quantile or density estimates across independent chains and making a judgement as to whether the ensemble of chains has converged to the distributional target. The main limitations of convergence diagnostics are (a) they detect some aspects of non-convergence, but do not provide a guarantee that convergence has occurred; (b) they typically make (e.g. Gaussian) assumptions on the target distribution that might not hold; (c) in taking  $b$  large enough to make bias negligible, the number  $n - b$  of remaining samples may be rather small, such that the statistical efficiency of the estimator in (3) is sub-optimal as an approximation of  $P$ . Nonetheless, a considerable portion of Bayesian pedagogy is devoted to the identification of the burn-in period, as facilitated using diagnostic tests that are built into commercial-grade software such as **WinBUGS** (Lunn et al., 2000), **JAGS** (Plummer, 2003), **R** (R Core Team, 2020), **Stan** (Carpenter et al., 2017). Some commonly-used convergence diagnostics are discussed in Section 2.1.

**Error Assessment:** The utility of an estimator for (1) is limited unless it is accompanied by a reliable assessment of its error. Theoretical considerations motivate the asymptotic variance (when it exists) as the basis for assessing the error of (2), once a function  $f$  of interest has been fixed (see e.g. Geyer, 1992; Tierney, 1994; Jones and Hobert, 2001; Atchadé et al., 2016; Rosenthal, 2017). However, approximation of asymptotic variance is typically at least as difficult as approximation of (1), typically relying on batch means estimators, spectral means estimators, or initial sequence estimators; see the recent reviews in Vats et al. (2019b); Roy (2019). A pragmatic approach to this problem is to restrict attention to a subset  $(X_{\pi(j)})_{j=1}^m$  of the MCMC output such that  $X_{\pi(j)}$  and  $X_{\pi(j')}$  are approximately independent whenever  $j \neq j'$ . This allows standard techniques from Monte Carlo to be approximately used in the context of estimators such as (3). In particular, approximate confidence intervals for (1) that are centred on (3) can be based on the sample variance of  $(f(X_{\pi(j)}))_{j=1}^m$ .

It is often stated that discarding part of the MCMC output leads to a reduction in the statistical efficiency of the estimator (3) compared to (2). This argument, made e.g. in Geyer (1992), applies only when the procedure used to discard part of the MCMC output does not itself depend on the MCMC output and when the length  $n$  of the MCMC output is fixed. That estimation efficiency can be *improved* by discarding a portion of the samples in a way that depends on the samples themselves is in fact well-established (see e.g. Dwivedi et al., 2019). Even if the procedure used to discard part of the MCMC output does not depend on the samples, it is still possible to improve estimation efficiency by discarding part of the MCMC output. Indeed, if the length  $n$  is just one factor to be optimised in the context of a finite computational budget then the estimator (3) may in fact be *more* accurate than (2), as we discuss next.

**Compression of MCMC Output:** A third motivation for estimators of the form (3) comes from the case where evaluation of  $f$ , or storage of the output of  $f$ , is associated with a considerable computational cost. In such situations one may want to control the cardinality

$m$  of the index set  $\pi$  in order that computation of (3) is practical. The standard solution to this problem is to retain only every  $t^{\text{th}}$  state visited by the Markov chain, where  $t = n/m$  and  $n$  is a multiple of  $m$ , in order that statistical dependence is reduced between the remaining states  $(X_{tj})_{j=1}^m$ . This procedure is known as “thinning” of the MCMC output. Owen (2017), considered the problem of how to optimally allocate a computational budget that can be used either to perform additional iterations of MCMC (i.e. larger  $n$ ) or to evaluate  $f$  on the MCMC output (i.e. larger  $m$ ). His analysis provides a recommendation on how  $t$  should be selected, as a function of the relative cost of the two computational operations that can be performed. In particular, he demonstrates that (3) can be more efficient than (2) in the context of a fixed computational budget, and when the Markov chain autocorrelation is monotonically decreasing and nonnegative.

The approaches to selection of an index set  $\pi$  just described are based on the identification of a suitable burn-in period  $b$  and/or a suitable thinning frequency  $t$ , and constitute the most popular approaches to constructing an estimator of the form (3). Nevertheless, the interplay between the Markov chain sample path and the heuristics used to select  $b$  and  $t$  is not widely appreciated. In general it is unclear how much bias may be introduced by employing a post-processing heuristic that is itself based on the MCMC output. Indeed, even the basic question of when the post-processed estimator in (3) is consistent appears not to have been studied.

In this paper we propose a novel method, called **Stein Thinning**, that selects an index set  $\pi$  of specified cardinality  $m$  such that the associated empirical approximation is close to optimal. This is achieved in such a way that the estimator (3) still constitutes a consistent approximation of (1); in fact, we establish the stronger result that the (random) empirical measure produced by **Stein Thinning** (almost surely) converges weakly to  $P$ . To achieve this we adopt a kernel Stein discrepancy as our optimality criterion, following Liu and Lee (2017); Chwialkowski et al. (2016); Gorham and Mackey (2017). The minimisation of kernel Stein discrepancy is performed using a greedy sequential algorithm and the main contribution of our theoretical analysis is to study the interplay of the greedy algorithm with the randomness inherent to the MCMC output. The proposed **Stein Thinning** method is extremely simple (see Algorithm 1), applicable to most problems where gradients of the posterior density can be computed, and implemented as convenient **Python** and **MATLAB** packages that require no additional user input other than the number  $m$  of states to be selected (see Appendix B).

## 1.1 Related Work

The topic of developing convergence diagnostics for MCMC has a rich literature and will be described in more detail in Section 2.

Our work contributes to an active area of research that attempts to cast empirical approximation as an optimisation problem. Liu and Lee (2017) considered the use of kernel Stein discrepancy to optimally weight an arbitrary set  $(X_i)_{i=1}^n \subset \mathbb{R}^d$  of states in a manner loosely analogous to importance sampling, at a computational cost of  $O(n^3)$ . The combined

effect of applying the approach of Liu and Lee (2017) to MCMC output was analysed in Hodgkinson et al. (2020), who established situations in which the overall procedure will be consistent. The present paper differs from Liu and Lee (2017) and Hodgkinson et al. (2020) in that we attempt compression, rather than weighting of the MCMC output. Thus, although **Stein Thinning** also attempts to minimise a kernel Stein discrepancy, the algorithm that we propose and analyse is of a fundamentally different nature to that considered in previous work, and addresses a different computational task. In principle one could use the algorithm of Liu and Lee (2017) to assign a weight  $w_i$  to each  $X_i$  and then retain the  $m$  states with largest absolute weights, but this entails a  $O(n^3)$  computational cost which is potentially far larger than the  $O(nm^2)$  computational cost of **Stein Thinning** and, furthermore, the mathematical justification for discarding states with small absolute weights has not been established.

If a compressed representation of the posterior  $P$  is required, but one is not wedded to the use of MCMC for generation of candidate states, then several other methods can be used. Joseph et al. (2015, 2019) proposed a criterion to capture how well an empirical measure based on a point set approximates  $P$  and then applied a global numerical optimisation method to arrive at a suitable point set (called a “minimum energy design”; MED). A similar approach was taken in Chen et al. (2018), where a kernel Stein discrepancy was numerically minimised (called “Stein points”; SP). The reliance on global optimisation renders the theoretical analysis of MED and SP difficult. In Chen et al. (2019) the authors considered using Markov chains to approximately perform numerical optimisation in the context of SP, allowing a tractable analytic treatment at the expense of a sub-optimal compression of  $P$ . Mak and Joseph (2018) considered selecting a small number of states to minimise a particular energy functional that quantifies the extent to which an empirical measure supported on those states approximates  $P$  (called “support points”). Their analysis covered the case of the optimal point set, but did not extend to the numerical methods used to approximately compute it. Liu and Wang (2016); Liu (2017) identified a gradient flow with  $P$  as a fixed point that can be approximately simulated using a particle method (called “Stein variational gradient descent”; SVGD) based on a relatively small number of particles. At convergence, one obtains a compressed representation of  $P$ , however the theoretical analysis of SVGD remains an open and active research topic (see e.g. Duncan et al., 2019). The present paper differs from the contributions cited in this paragraph, in that (1) our algorithm requires only the output from one run of MCMC, which is a realistic requirement in many situations, and (2) we are able to provide a finite sample size error bound (Theorem 2) and a consistency guarantee (Corollary 1) for **Stein Thinning**, that cover precisely the algorithm that we implement.

## 1.2 Outline of the Paper

The paper proceeds, in Section 2, to recall the standard approaches used to post-process MCMC output. In Section 3 we present **Stein Thinning** and establish a finite sample size error bound, as well as a widely-applicable consistency result. In Section 4 we present an extensive empirical assessment of **Stein Thinning** in the context of parameter inference

for challenging ordinary differential equation models. Our motivation for this work comes from a problem in which we must infer a 38-dimensional parameter in a calcium signalling model, defined by a stiff system of 6 coupled differential equations, where scientific quantities of interest  $f$  involve high-fidelity simulations from the dynamical system in a multi-scale and multi-physics model of the human heart. There, the computational cost associated with evaluation of  $f$  is comparable with that of obtaining MCMC output and therefore compression of the MCMC output is essential. Conclusions are contained in Section 5.

## 2 Background

Below we recall how selection of the index set  $\pi$  in (3) would typically be performed. As discussed in the introduction, the standard practice in applications of MCMC is to identify a burn-in period  $b$ , and possibly also a thinning parameter  $t$  if compression is required, leading to an empirical approximation

$$\hat{P} := \frac{1}{\lfloor (n-b)/t \rfloor} \sum_{i=1}^{\lfloor (n-b)/t \rfloor} \delta(x_{b+it}).$$

Here  $\lfloor r \rfloor$  denotes the integer part of  $r$  and  $\delta(x)$  is a point mass centred at  $x \in \mathbb{R}^d$ . This corresponds to a set of indices  $\pi$  in (3) that discards the burn-in states and retains only every  $t^{\text{th}}$  iteration from the remainder of the MCMC output. It includes the case where no states are removed when  $b = 0$  and  $t = 1$ . In Section 2.1 we discuss commonly used heuristics for selecting  $b$  and in Section 2.2 we discuss how  $t$  might be selected.

### 2.1 Using Convergence Diagnostics to Select $b$

Convergence diagnostics are widely used to test for non-convergence of MCMC. Their use is limited to reducing bias in MCMC output; they are not optimised for the fixed  $n$  setting, which requires a bias-variance trade-off. Nevertheless, convergence diagnostics constitute the principal means by which MCMC output is post-processed. Here we summarise the widely-used diagnostics of Gelman and Rubin (1992); Brooks and Gelman (1998); Gelman et al. (2014) (the *GR diagnostic*), as well as the more recent work of Vats and Knudson (2018) (the *VK diagnostic*).

The GR diagnostic is based on running  $L$  independent chains, each of length  $n$ , with starting points that are over-dispersed with respect to the target distribution. Obtaining initial points with such characterisation is not trivial because the target is not known beforehand; we refer to the original literature for advice on how to select these initial points, but, in practice, it is not uncommon to guess them. When the support of the target distribution is uni-dimensional (or when  $d > 1$ , but only a uni-dimensional marginal is used), the GR diagnostics ( $\hat{R}^{\text{GR},L}$ ) is obtained as the square root of the ratio of two estimators of the

variance  $\sigma^2$  of the target. In particular,

$$\hat{R}^{\text{GR},L} := \sqrt{\frac{\hat{\sigma}^2}{s^2}}, \quad (4)$$

where  $s^2$  is the (arithmetic) mean of the sample variances  $s_l^2$ ,  $l = 1, \dots, L$ , of the chains, which typically provides an underestimate of  $\sigma^2$ , and  $\hat{\sigma}^2$  is constructed as an overestimate of the target variance

$$\hat{\sigma}^2 := \frac{n-1}{n} s^2 + \frac{B}{n},$$

where the term  $B/n$  is an estimate of for the asymptotic variance of the sample mean of the Markov chain. In the original GR diagnostics, this asymptotic variance was estimated as the sample variance of the means  $\bar{X}_l$ ,  $l = 1, \dots, L$ , from the  $L$  chains, leading to

$$\frac{B}{n} = \frac{1}{L-1} \sum_{l=1}^L \left( \bar{X}_l - \frac{1}{L} \sum_{l'=1}^L \bar{X}_{l'} \right)^2.$$

The improved VK diagnostic,  $\hat{R}^{\text{VK},L}$ , is formally obtained in the same way as (4), but with more efficient estimators  $\tau^2/n$  for the asymptotic variance used in place of  $B/n$ . A number of options are available here, but the (luggsail) batch mean estimator of Vats and Flegal (2018) is recommended because it is guaranteed to be biased from above, while still being consistent (in our simulations we use batches of size  $\sqrt[3]{n}$ ). This gain in efficiency leads to improved performance of the VK diagnostic over the GR diagnostic, in the sense that it is less sensitive to the randomness in the Markov chains and the number of chains used. In particular,  $\hat{R}^{\text{VK},L}$  can be computed using one chain only ( $L = 1$ ), which has clear practical appeal.

For an ergodic Markov chain,  $\hat{R}^{\text{GR},L}$  and  $\hat{R}^{\text{VK},L}$  converge to 1 as  $n \rightarrow \infty$ , so that selection of a suitable burn-in period  $b$  amounts to observing when these diagnostics are below  $1 + \delta$ , where  $\delta$  is a suitable threshold. In the literature on  $\hat{R}^{\text{GR},L}$ , the somewhat arbitrary choice  $\delta = 0.1$  is commonly used, see Gelman et al. (2014, Ch. 11.5) and the survey in Vats and Knudson (2018). In the literature on  $\hat{R}^{\text{VK},L}$ , Vats and Knudson (2018) showed how  $\delta$  can be selected by exploiting the relationship between  $\hat{R}^{\text{VK},L}$  and the effective sample size (ESS) when estimating the mean of the target. In particular, it is possible to re-write

$$\hat{R}^{\text{VK},L} = \sqrt{\left( \frac{n-1}{n} \right) + \frac{L}{\widehat{\text{ESS}}}} \quad (5)$$

where  $\widehat{\text{ESS}}$  is a strongly consistent estimator of the ESS. One can therefore (approximately) select a  $\delta$  threshold that corresponds to a pre-specified value of the ESS. The literature on error assessment for MCMC provides guidance on how large the ESS ought to be in order

that a  $(1 - \alpha)\%$  confidence interval for (1), centred at (2), is below a specified threshold  $\epsilon$ ; see Jones and Hobert (2001); Flegal et al. (2008); Vats et al. (2019a):

$$\widehat{\text{ESS}} \geq M_{\alpha, \epsilon} := \frac{2^2 \pi}{(\Gamma(1/2))^2} \frac{\chi_{1-\alpha}^2}{\epsilon^2}, \quad (6)$$

where  $\Gamma(\cdot)$  is the Gamma function,  $\chi_{1-\alpha}^2$  is the  $(1 - \alpha)^{\text{th}}$  quantile of the  $\chi^2$  distribution with one degree of freedom. Plugging (6) in (5) leads to the conclusion that, after the first iteration for which  $\hat{R}^{\text{VK},L}$  is below  $1 + \delta$ , where

$$\delta \equiv \delta(L, \alpha, \epsilon) = \sqrt{1 + \frac{L}{M_{\alpha, \epsilon}}} - 1, \quad (7)$$

the chain will provide estimators of the (marginal) means with small Monte Carlo error, when compared to the variability of the target distribution. The default choices  $\alpha = 0.05$  and  $\epsilon = 0.05$  were suggested in Vats and Knudson (2018), and were assumed in the sequel. For experiments reported in this paper we used (7) to select an appropriate threshold for both  $\hat{R}^{\text{GR},L}$  and  $\hat{R}^{\text{VK},L}$ , which leads to the burn-in periods that we denote  $\hat{b}^{\text{GR},L}$ , and  $\hat{b}^{\text{VK},L}$ , respectively.

The above discussion focussed on the univariate case, but generalisations of these convergence diagnostics are available and can be found in Brooks and Gelman (1998) and Vats and Knudson (2018). All convergence diagnostics in this work were computed using the R packages `coda` (Plummer et al., 2006) and `stableGR` (Knudson and Vats, 2020). The GR diagnostic in the software package uses the original definition in Gelman and Rubin (1992), that differs slightly from (4); however, this difference is not expected to strongly affect the discussion above nor the simulation results in Section 4.

## 2.2 Approaches to Selection of $t$

Thinning is often employed when compression of MCMC output is required. One motivating example is provided by the calcium signalling model that we discuss in Section 4.4. Despite the widespread use of thinning, only quite basic strategies are employed. For the experimental assessment in this paper we will report approximation quality as  $m$  is increased, and we therefore define three distinct strategies for thinning that each produce a sequence of index sets  $\pi$  of cardinalities 1 to  $m$  from fixed MCMC output:

- (i) Fixed lag:  $t = \lfloor (n - b)/m \rfloor$ , where  $m$  is the total number of points to obtain. Index sets produced in this way are nested.
- (ii) Fixed number of points:  $t = \lfloor (n - b)/m' \rfloor$ , for  $m' = 1, \dots, m$ . Index sets produced in this way are not nested.
- (iii) Consecutive points:  $t = 1$ . Index sets produced in this way are nested.

The final index set, of cardinality  $m$ , produced by (i) and (ii) will be identical. Strategy (iii) represents the situation where no thinning is performed.

This completes our discussion of background material. Next we present our proposed **Stein Thinning** method.

### 3 Methods

In this section we introduce and analyse the **Stein Thinning** method. First, in Section 3.1, we recall the construction of a kernel Stein discrepancy and its theoretical properties. The **Stein Thinning** method is presented in Section 3.2 and theoretical analysis is provided in Section 3.3. Section 3.4 is devoted to details of how **Stein Thinning** is implemented.

Before we proceed, we highlight the following standing assumption:

**Standing Assumption:** Throughout we assume that the distributional target  $P$  admits a positive and continuously differentiable density  $p$  on  $\mathbb{R}^d$ .

#### 3.1 Kernel Stein Discrepancy

To construct a criterion for the selection of states from the MCMC output, we require a notion of optimal approximation for probability distributions. To this end, recall the notion of an *integral probability metric* (IPM) (Muller, 1997) based on a set  $\mathcal{F}$  of measure-determining functionals on  $\mathbb{R}^d$ , defined as

$$D_{\mathcal{F}}(P, Q) := \sup_{f \in \mathcal{F}} \left| \int_{\mathbb{R}^d} f dP - \int_{\mathbb{R}^d} f dQ \right|. \quad (8)$$

The fact that  $\mathcal{F}$  is measure-determining means that  $D_{\mathcal{F}}(P, Q) = 0$  if and only if  $P = Q$  is satisfied. Standard choices for  $\mathcal{F}$ , e.g. that recover Wasserstein distance as the IPM, cannot be used in the Bayesian context due to the need to compute integrals with respect to  $P$  in (8). To circumvent this issue, the notion of a *Stein discrepancy* was proposed in Gorham and Mackey (2015). This was based on Stein's method (Stein, 1972), which consists of finding a differential operator  $\mathcal{A}_P$ , depending on  $P$  and acting on  $d$ -dimensional vector fields on  $\mathbb{R}^d$ , and a set  $\mathcal{G}$  of sufficiently differentiable  $d$ -dimensional vector fields on  $\mathbb{R}^d$  such that  $\int_{\mathbb{R}^d} \mathcal{A}_P g dP = 0$  for all  $g \in \mathcal{G}$ . The proposal of Gorham and Mackey (2015) was to take  $\mathcal{F} = \mathcal{A}_P \mathcal{G}$  to be the image of  $\mathcal{G}$  under  $\mathcal{A}_P$  in (8), leading to the *Stein discrepancy*

$$D_{\mathcal{A}_P \mathcal{G}}(P, Q) = \sup_{g \in \mathcal{G}} \left| \int_{\mathbb{R}^d} \mathcal{A}_P g dQ \right|. \quad (9)$$

Theoretical analysis had led to sufficient conditions for  $\mathcal{A}_P \mathcal{G}$  to be measure-determining (Gorham and Mackey, 2015). In this paper we focus on a particular form of (9) due to Liu et al. (2016); Chwialkowski et al. (2016), called a *kernel Stein* discrepancy (KSD). In this case  $\mathcal{A}_P$  is the *canonical Stein operator*

$$\mathcal{A}_P g := \frac{1}{p} \nabla \cdot (pg),$$

where  $\nabla$  denotes the divergence operator in  $\mathbb{R}^d$  and  $\mathcal{G}$  is the unit ball in a Cartesian product of reproducing kernel Hilbert spaces

$$\mathcal{G} := \left\{ g : \mathbb{R}^d \rightarrow \mathbb{R}^d \left| \sum_{i=1}^d \|g_i\|_{\mathcal{H}(k)}^2 \leq 1 \right. \right\},$$

where we recall that a reproducing kernel Hilbert space (RKHS)  $\mathcal{H}(k)$  of functionals on  $\mathbb{R}^d$  is a Hilbert space with inner product denoted  $\langle \cdot, \cdot \rangle_{\mathcal{H}(k)}$ , equipped with a function  $k : \mathbb{R}^d \times \mathbb{R}^d \rightarrow \mathbb{R}$ , called a *kernel*, such that  $\forall x \in \mathbb{R}^d$  we have  $k(\cdot, x) \in \mathcal{H}(k)$  and  $\forall x \in \mathbb{R}^d, h \in \mathcal{H}(k)$  we have  $h(x) = \langle h, k(\cdot, x) \rangle_{\mathcal{H}(k)}$  (Berlinet and Thomas-Agnan, 2004). It follows from construction that the set  $\mathcal{A}_P \mathcal{G}$  is the unit ball of another RKHS, denoted  $\mathcal{H}(k_P)$ , whose kernel is

$$\begin{aligned} k_P(x, y) := & \nabla_x \cdot \nabla_y k(x, y) + \langle \nabla_x k(x, y), \nabla_y \log p(y) \rangle \\ & + \langle \nabla_y k(x, y), \nabla_x \log p(x) \rangle + k(x, y) \langle \nabla_x \log p(x), \nabla_y \log p(y) \rangle, \end{aligned} \quad (10)$$

where  $\langle \cdot, \cdot \rangle$  denotes the standard Euclidean inner product,  $\nabla$  denotes the gradient operator and subscripts have been used to indicate the variables being acted on by the differential operators (Oates et al., 2017). Thus KSD is recognised as a maximum mean discrepancy in  $\mathcal{H}(k_P)$  (Gretton et al., 2006) and is fully characterised by the kernel  $k_P$ ; we therefore adopt the shorthand notation  $D_{k_P}(Q)$  for  $D_{\mathcal{A}_P \mathcal{G}}(P, Q)$ .

In the remainder of this section we recall the main properties of KSD. The first is a condition on the kernel  $k$  that guarantees elements of  $\mathcal{H}(k_p)$  have zero mean with respect to  $P$ . In what follows  $\|x\| = \langle x, x \rangle^{1/2}$  denotes the Euclidean norm on  $\mathbb{R}^d$ . It will be convenient to abuse operator notation, writing  $\nabla_x \nabla_y^\top k$  for the Hessian matrix of a bivariate function  $(x, y) \mapsto k(x, y)$ .

**Proposition 1** (Proposition 1 of Gorham and Mackey (2017)). *Let  $(x, y) \mapsto \nabla_x \nabla_y^\top k(x, y)$  be continuous and uniformly bounded on  $\mathbb{R}^d$  and let  $\int_{\mathbb{R}^d} \|\nabla \log p\| dP < \infty$ . Then  $\int_{\mathbb{R}^d} h dP = 0$  for all  $h \in \mathcal{H}(k_P)$ , where  $k_P$  is defined in (10).*

The second main property of KSD that we will need is that it can be explicitly computed for an empirical measure  $Q = \frac{1}{n} \sum_{i=1}^n \delta(x_i)$ , supported on states  $x_i \in \mathbb{R}^d$ :

**Proposition 2** (Proposition 2 of Gorham and Mackey (2017)). *Let  $(x, y) \mapsto \nabla_x \nabla_y k(x, y)$  be continuous on  $\mathbb{R}^d$ . Then*

$$D_{k_P} \left( \frac{1}{n} \sum_{i=1}^n \delta(x_i) \right) = \sqrt{\frac{1}{n^2} \sum_{i,j=1}^n k_P(x_i, x_j)}, \quad (11)$$

where  $k_P$  was defined in (10).

The third main property is that KSD provides convergence control. Let  $Q_n \Rightarrow P$  denote weak convergence of a sequence  $(Q_n)$  of measures to  $P$ . Theoretical analysis in (Gorham and Mackey, 2017; Chen et al., 2018; Huggins and Mackey, 2018; Chen et al., 2019; Hodgkinson et al., 2020) established sufficient conditions for when convergence of (11) to zero implies  $\frac{1}{n} \sum_{i=1}^n \delta(x_i) \Rightarrow P$ . For our purposes we present one such result, from Chen et al. (2019).

**Proposition 3** (Theorem 4 in Chen et al. (2019)). *Let  $P$  be distantly dissipative, meaning that  $\liminf_{r \rightarrow \infty} \kappa(r) > 0$  where*

$$\kappa(r) := \inf \left\{ -2 \frac{\langle \nabla_x \log p(x) - \nabla \log p(y), x - y \rangle}{\|x - y\|^2} : \|x - y\| = r \right\}.$$

*Consider the kernel  $k(x, y) = (c^2 + \|\Gamma^{-1/2}(x - y)\|^2)^\beta$  for some fixed  $c > 0$ , a fixed positive definite matrix  $\Gamma$  and a fixed exponent  $\beta \in (-1, 0)$ . Then*

$$D_{k_P} \left( \frac{1}{n} \sum_{i=1}^n \delta(x_i) \right) \rightarrow 0 \quad \text{implies} \quad \frac{1}{n} \sum_{i=1}^n \delta(x_i) \implies P,$$

where  $k_P$  is defined in (10).

The properties just described ensure that KSD is a suitable optimality criterion to consider for the post-processing of MCMC output. Our attention turns next to the development of algorithms for minimisation of KSD.

### 3.2 Greedy Minimisation of KSD

The convergence control afforded by Proposition 3 motivates the design of methods that select points  $(x_i)_{i=1}^n$  in  $\mathbb{R}^d$  such that (11) is approximately minimised. Optimisation algorithms for this task were proposed in Chen et al. (2018) and Chen et al. (2019). In Chen et al. (2018), deterministic optimisation techniques were considered for low-dimensional problems, whereas in Chen et al. (2019) a Markov chain was used to provide more a practical optimisation strategy when the state space is high-dimensional. In each case greedy sequential strategies were considered, wherein at iteration  $n$  a new state  $x_n$  is appended to the current sequence  $(x_1, \dots, x_{n-1})$  by searching over a compact subset of  $\mathbb{R}^d$ . Chen et al. (2018) also considered the use of conditional gradient algorithms (so-called *Frank-Wolfe*, or *kernel herding* algorithms) but found that greedy algorithms provided better performance across a range of experiments and therefore we focus on greedy algorithms in this manuscript.

The present paper is distinguished from earlier work in that we do not attempt to solve a continuous optimisation problem for selection of the next point  $x_n \in \mathbb{R}^d$ . Such optimisation problems are fundamentally difficult and can at best be approximately solved. Instead, we exactly solve the discrete optimisation problem of selecting a suitable element  $x_n$  from a supplied MCMC output. In this sense we expect our findings will be more widely applicable than previous work, since we are simply performing post-processing of MCMC output and there exists a variety of commercial-grade software for MCMC. The method that we propose, called **Stein Thinning**, is straight-forward to implement and succinctly stated in Algorithm 1. (The convention  $\sum_{i=1}^0 = 0$  is employed.)

The algorithm is illustrated on a simple bivariate Gaussian mixture model in Figure 1. Observe in this figure that the points selected by the **Stein Thinning** do not belong to the burn-in period (which is visually clear), and that although the MCMC spent a disproportionate amount of time in one of the mixture components, the number of points selected by

**Data:** The output  $(x_i)_{i=1}^n$  from an MCMC method, a kernel  $k_P$ , such as in (10), and a desired cardinality  $m \in \mathbb{N}$ .

**Result:** The indices  $\pi$  of a sequence  $(x_{\pi(j)})_{j=1}^m \subset \{x_i\}_{i=1}^n$  where the  $\pi(j)$  are elements of  $\{1, \dots, n\}$ .

**for**  $j = 1, \dots, m$  **do**

$$\pi(j) \in \arg \min_{i=1, \dots, n} \frac{k_P(x_i, x_i)}{2} + \sum_{j'=1}^{j-1} k_P(x_{\pi(j')}, x_i);$$

**end**

**Algorithm 1:** The proposed method; **Stein Thinning**.

**Stein Thinning** is approximately equal across the two components of the target. A detailed empirical assessment is presented in Section 4.

**Remark 1.** *In the event of a tie, some additional tie-breaking rule should be used to select the next index. For example, if the minimum in Algorithm 1 is realised by multiple candidate values  $\Pi(j) \subseteq \{1, \dots, n\}$ , one could adopt a tie-breaking rule that selects the smallest element of  $\Pi(j)$  as the value that is assigned to  $\pi(j)$ . The rule that is used has no bearing on our theoretical analysis in Section 3.3.*

**Remark 2.** *The computation associated with iteration  $j$  of Algorithm 1 is  $O(nj)$  and therefore the computational complexity of Algorithm 1 is  $O(nm^2)$ . For typical MCMC algorithms the computational complexity is  $O(n)$ , so the computational complexity of **Stein Thinning** is equal to that for MCMC when  $m$  is fixed and higher when  $m$  is increasing with  $n$ . The storage requirement of **Stein Thinning** is  $O(nm)$ .*

**Remark 3.** *In general the indices in  $\pi$  need not be distinct. That is, Algorithm 1 may prefer to include a duplicate state rather than to include a state which is not useful for representing  $P$ . Indeed, if  $m > n$  then the sequence  $(x_{\pi(j)})_{j=1}^m$  must contain duplicates entries. Theorem 1 in Section 3.3 clarifies this behaviour.*

**Remark 4.** *The random variables  $X_{\pi(j)}$  are highly dependent by construction and this precludes even the approximate use of confidence intervals that are commonly employed with Monte Carlo estimators to assess the accuracy of (3) when **Stein Thinning** is used. However, we note that caching of the quantities computed during Algorithm 1 enables the KSD of the resulting empirical distribution to be computed. As explained in Section 4 of South et al. (2020), the KSD can form the basis of an approximate error bound for estimators of the form (3).*

### 3.3 Theoretical Analysis

The theoretical analysis in this section clarifies the limiting behaviour of **Stein Thinning** as  $m, n \rightarrow \infty$ . The arguments that we present hold for a distribution  $P$  defined on a general

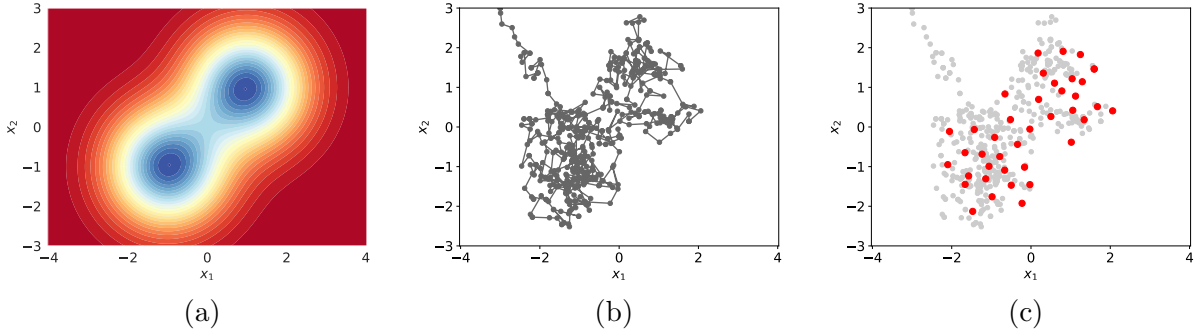


Figure 1: Illustration of **Stein Thinning**: (a) Contours of the distributional target  $P$ . (b) Markov chain Monte Carlo (MCMC) output, limited to 500 iterations to mimic a challenging computational context, exhibiting burn-in and autocorrelation that must be identified and mitigated. (c) A subset of  $m = 40$  states from the MCMC output selected using **Stein Thinning**, which correctly identifies and ignores the burn-in period and stratifies states equally across the two components of the target.

measurable space  $\mathcal{X}$ , and are presented as such, but the main focus of this paper is the case  $\mathcal{X} = \mathbb{R}^d$ . Our first main result concerns the behaviour of **Stein Thinning** on a fixed sequence  $(x_i)_{i=1}^n$ :

**Theorem 1.** *Let  $\mathcal{X}$  be a measurable space and let  $P$  be a probability distribution on  $\mathcal{X}$ . Let  $k_P : \mathcal{X} \times \mathcal{X} \rightarrow \mathbb{R}$  be a reproducing kernel with  $\int_{\mathcal{X}} k_P(x, \cdot) dP(x) = 0$  for all  $x \in \mathcal{X}$ . Let  $(x_i)_{i=1}^n \subset \mathcal{X}$  be fixed and consider an index sequence  $\pi$  of length  $m$  produced by Algorithm 1. Then we have the bound*

$$D_{k_P} \left( \frac{1}{m} \sum_{j=1}^m \delta(x_{\pi(j)}) \right)^2 \leq D_{k_P} \left( \sum_{i=1}^n w_i \delta(x_i) \right)^2 + \left( \frac{1 + \log(m)}{m} \right) \max_{i=1, \dots, n} k_P(x_i, x_i),$$

where the weights  $w = (w_1, \dots, w_n)$  in the first term satisfy

$$w \in \arg \min_{\substack{1_n^\top w = 1 \\ w \geq 0}} D_{k_P} \left( \sum_{i=1}^n w_i \delta(x_i) \right) \quad (12)$$

where  $1_n^\top = (1, \dots, 1)$  and  $w \geq 0$  indicates that  $w_i \geq 0$  for  $i = 1, \dots, n$ .

The proof of Theorem 1 is provided in Appendix A.1. Its implication is that, given a sequence  $(x_i)_{i=1}^n$ , **Stein Thinning** produces an empirical distribution that converges in KSD to the optimal weighted empirical distribution  $\sum_{i=1}^n w_i \delta(x_i)$  based on that sequence. Properties of such optimally weighted empirical measures were studied in Liu and Lee (2017); Hodgkinson et al. (2020), and are not the focus of the present paper, where the case  $m \ll n$  is of principal interest. The role of Theorem 1 is to provide a means to study the interaction between the greedy algorithm and a given sequence  $(x_i)_{i=1}^n$ , and this bound is central to Theorem 2 in the sequel.

**Remark 5.** The weights  $w$  in Theorem 1 can be computed using numerical optimisation by noting that the KSD is a quadratic function of  $w$  that is subject to a linear and a non-negativity constraint (Liu and Lee, 2017). If the non-negativity constraint is removed then an analytic calculation can be performed;

$$v = \arg \min_{\substack{1^\top v = 1}} D_{k_P} \left( \sum_{i=1}^n v_i \delta(x_i) \right) = \frac{K_P^{-1} 1_n}{1_n^\top K_P^{-1} 1_n}, \quad (K_P)_{i,j} := k_P(x_i, x_j),$$

whose derivation follows that described in Oates et al. (2017). The use of weighted measures is not discussed in much detail in the present paper since the condition number of the matrix  $K_P$  typically increases rapidly with  $n$ , meaning that additional regularisation is often required. Moreover, the computational cost associated with the solution of the linear system can be prohibitively large when  $n$  is greater than a few hundred. The use of optimal or sub-optimal weighting within each iteration of Stein Thinning may be interesting to explore, and we refer to Bach et al. (2012) for related work.

**Remark 6.** The use of a conditional gradient algorithm, instead of a greedy algorithm, in this context amounts to simply removing the term  $k_P(x_{\pi(j)}, x_{\pi(j)})$  in Algorithm 1. As discussed in Chen et al. (2018), this term can be thought of as a regulariser that lends stability to the algorithm, avoiding selection of  $x_i$  that are far from the effective support of  $P$ .

**Remark 7.** Theorem 1 is formulated at a high level of generality and can be applied on non-Euclidean domains  $\mathcal{X}$ . In Barp et al. (2018); Liu and Zhu (2018); Xu and Matsuda (2020); Le et al. (2020) the authors proposed and discussed Stein operators  $\mathcal{A}_P$  for the non-Euclidean context.

In what follows we consider the properties of Stein Thinning applied to MCMC output. Let  $V$  be a function  $V : \mathcal{X} \rightarrow [1, \infty)$  and, for a function  $f : \mathcal{X} \rightarrow \mathbb{R}$  and a measure  $\mu$  on  $\mathcal{X}$ , let

$$\|f\|_V := \sup_{x \in \mathcal{X}} \frac{|f(x)|}{V(x)}, \quad \|\mu\|_V := \sup_{\|f\|_V \leq 1} \left| \int_{\mathcal{X}} f d\mu \right|.$$

Recall that a Markov chain  $(X_i)_{i \in \mathbb{N}} \subset \mathcal{X}$  with  $n^{\text{th}}$  step transition kernel  $P^n$  is called  $V$ -uniformly ergodic (Meyn and Tweedie, 2012, Chap. 16) if  $\exists R \in [0, \infty), \rho \in (0, 1)$  such that

$$\|P^n(x, \cdot) - P\|_V \leq RV(x)\rho^n \tag{13}$$

for all initial states  $x \in \mathcal{X}$  and all  $n \in \mathbb{N}$ . The notation  $\mathbb{E}$  will be used to denote expectation with respect to the law of the Markov chain in the sequel. Our main result, Theorem 2, establishes a finite sample size error bound for Stein Thinning applied to MCMC output:

**Theorem 2.** Let  $\mathcal{X}$  be a measurable space and let  $P$  be a probability distribution on  $\mathcal{X}$ . Let  $k_P : \mathcal{X} \times \mathcal{X} \rightarrow \mathbb{R}$  be a reproducing kernel with  $\int_{\mathcal{X}} k_P(x, \cdot) dP(x) = 0$  for all  $x \in \mathcal{X}$ . Consider a  $P$ -invariant time-homogeneous reversible Markov chain  $(X_i)_{i \in \mathbb{N}} \subset \mathcal{X}$  generated using a

$V$ -uniformly ergodic transition kernel, such that (13) is satisfied with  $V(x) \geq \sqrt{k_P(x, x)}$  for all  $x \in \mathcal{X}$ . Suppose that, for some  $\gamma > 0$ ,

$$b := \sup_{i \in \mathbb{N}} \mathbb{E} [e^{\gamma k_P(X_i, X_i)}] < \infty, \quad M := \sup_{i \in \mathbb{N}} \mathbb{E} [\sqrt{k_P(X_i, X_i)} V(X_i)] < \infty.$$

Let  $\pi$  be an index sequence of length  $m$  produced by Algorithm 1 applied to the Markov chain output  $(X_i)_{i=1}^n$ . Then, with  $C = \frac{2R\rho}{1-\rho}$ , we have that

$$\mathbb{E} \left[ D_{k_P} \left( \frac{1}{m} \sum_{j=1}^m \delta(X_{\pi(j)}) \right)^2 \right] \leq \frac{\log(b)}{\gamma n} + \frac{CM}{n} + \left( \frac{1 + \log(m)}{m} \right) \frac{\log(nb)}{\gamma}. \quad (14)$$

That convergence in mean does not imply almost sure convergence motivates us to strengthen the conclusion of Theorem 2 in Corollary 1, which establishes an almost sure convergence guarantee for **Stein Thinning**:

**Corollary 1.** *Under the assumptions of Proposition 3 and Theorem 2, if  $m \leq n$  and the growth of  $n$  is limited to at most  $\log(n) = O(m^{\beta/2})$  for some  $\beta < 1$ , then*

$$\frac{1}{m} \sum_{j=1}^m \delta(X_{\pi(j)}) \implies P$$

almost surely as  $m, n \rightarrow \infty$ .

The proofs of Theorem 2 and Corollary 1 are provided in Appendix A.2. The implication of Theorem 2 is that **Stein Thinning** provides a consistent approximation of  $P$  as quantified by KSD in the limit  $m, n \rightarrow \infty$ . Thus, if the conditions of Proposition 3 are also satisfied, Corollary 1 implies that the output of **Stein Thinning** almost surely converges weakly to  $P$ .

**Remark 8.** *The upper bound in (14) is asymptotically minimised when  $m \asymp n$ , however if  $m$  is comparable to  $n$  then no compression of the MCMC output is achieved. In practice we are interested in the case where values of  $m \ll n$  being used. It is not claimed that the bound in (14) is tight and indeed empirical results in Section 4 endorse the use of **Stein Thinning** in the small  $m$  context.*

**Remark 9.** *For  $\mathcal{X} = \mathbb{R}^d$  and  $k_P$  in (10), based on a radial kernel  $k$  in (10), meaning that  $k(x, y) = \phi(x - y)$  for some function  $\phi : \mathbb{R}^d \rightarrow \mathbb{R}$  satisfying  $\nabla \phi(0) = 0$ , we have that*

$$k_P(x, x) = -\Delta \phi(0) + \phi(0) \|\nabla \log p(x)\|^2.$$

*The function  $x \mapsto \sqrt{k_P(x, x)}$  appearing in the preconditions of Theorem 2 can therefore be understood in terms of  $\|\nabla \log p(x)\|$ . Results on the  $V$ -uniform ergodicity of Markov chains, which relate to the pre-conditions of Theorem 2, were discussed in Chen et al. (2019).*

### 3.4 Choice of Kernel

The suitability of KSD to quantify how well  $Q$  approximates  $P$  is determined by the choice of the kernel  $k$  in (10). Several choices are possible and, based on Proposition 3 together with extensive empirical assessment, Chen et al. (2019) advocated the use of the following pre-conditioned inverse multi-quadric kernel

$$k(x, y) := (1 + \|\Gamma^{-1/2}(x - y)\|^2)^{-1/2}$$

where, compared to Proposition 3, we have fixed  $c = 1$  (without loss of generality) and  $\beta = -1/2$ . The positive definite matrix  $\Gamma$  remains to be specified and it is natural to take a data-driven approach where the MCMC output is used to select  $\Gamma$ . Provided that a fixed number  $n_0 \in \mathbb{N}$  of the states  $(X_i)_{i=1}^{n_0}$  from the MCMC output are used in the construction of  $\Gamma$ , consistency of Stein Thinning is not affected. To explore different strategies for the selection of  $\Gamma$ , in Section 4 we assess the following candidates:

- **Median heuristic (med):** The scaled identity matrix  $\Gamma = \ell^2 I$ , where

$$\ell = \text{med} := \text{median}\{\|X_i - X_j\| : 1 \leq i < j \leq n_0\}$$

is the median Euclidean distance between states (Garreau et al., 2018). In the rare case that  $\text{med} = 0$ , an exception should be used, such as  $\ell = 1$ , to ensure a positive definite  $\Gamma$  is used.

- **Scaled median heuristic (sclmed):** The heuristic  $\Gamma = \ell^2 I$ , where

$$\ell = \text{med}/\sqrt{\log(m)}.$$

This was proposed in the context of Stein variational gradient descent in Liu and Wang (2016) and arises from the intuition that  $\sum_{j'=1}^m k_P(x_{\pi(j)}, x_{\pi(j')}) \approx m \exp(-\ell^{-2} \text{med}^2) = 1$ . Note the dependence on  $m$  means that the preceding theoretical analysis does not apply when this heuristic is used.

- **Sample covariance (smpcov):** The matrix  $\Gamma$  was taken equal to the sample covariance matrix  $S$  where

$$S = \frac{1}{n_0 - 1} \sum_{i=1}^{n_0} (X_i - \bar{X}) (X_i - \bar{X})^\top, \quad \bar{X} := \frac{1}{n_0} \sum_{i=1}^{n_0} X_i,$$

provided that this matrix is non-singular. As with the median heuristic, an exception should be used when  $S$  is singular, to ensure that a positive definite  $\Gamma$  is used.

- **Bayesian learning (bayesian):** Under the crude approximation that the  $X_i$  are independent draws from a Gaussian  $\mathcal{N}(\mu, \Sigma)$  with unknown mean  $\mu$  and covariance  $\Sigma$ , a

conjugate Bayesian approach to jointly estimate  $\mu$  and  $\Sigma$  starts with a normal-inverse-Wishart distribution  $(\mu, \Sigma) \sim \mathcal{NIW}(\mu_0, \lambda, \Psi, \nu)$  and leads to a conjugate normal-inverse-Wishart posterior  $(\mu, \Sigma) | (X_i)_{i=1}^{n_0} \sim \mathcal{NIW}(\mu_{n_0}, \lambda_{n_0}, \Psi_{n_0}, \nu_{n_0})$ , the mean of which for  $\Sigma$  is

$$\frac{\Psi_{n_0}}{\nu_{n_0} - d - 1} = \frac{1}{\nu + n_0 - d - 1} \left( \Psi + (n_0 - 1)S + \frac{\lambda n_0}{\lambda + n_0} (\bar{X} - \mu_0)(\bar{X} - \mu_0)^\top \right). \quad (15)$$

See p73 of Gelman et al. (2014) for the formulae for  $\mu_{n_0}$ ,  $\lambda_{n_0}$ ,  $\Psi_{n_0}$  and  $\nu_{n_0}$ . If one has access to suitable choices for  $\mu_0$ ,  $\lambda_0$ ,  $\Psi_0$  and  $\nu_0$ , perhaps from contextual information about  $P$ , then these can be used. Otherwise, we consider taking  $\Gamma$  equal to (15) under the default choices  $\mu_0 = 0$ ,  $\lambda = 0$ ,  $\Psi = I$  and  $\nu = 0$ , which amounts to a naively regularised sample covariance matrix. Note that the regularisation means positive definiteness of  $\Gamma$  is guaranteed.

- **Average Hessian (avehess):** The Hessian matrix of  $p$  at its mode could provide a suitable notion of curvature that could be used to construct  $\Gamma$ . Unfortunately, for the ODE problems that motivate this work, the computation of second order sensitivities is rarely convenient. As an alternative, the identity

$$-\mathbb{E}[\nabla \nabla^\top \log p(X)] = \mathbb{E}[\nabla \log p(X) \nabla \log p(X)^\top]$$

suggests taking

$$\Gamma^{-1} = \frac{1}{n_0} \sum_{i=1}^{n_0} \nabla \log p(X_i) \nabla \log p(X_i)^\top. \quad (16)$$

The latter has the advantage of requiring first order gradient information only. In the event that (16) is singular, an exception should again be used.

The experiments in Section 4 shed light on which of these heuristics is the most effective in practice. In what follows, we set  $n_0 = \min(n, 10^3)$  for the median and scaled median heuristic, to avoid an  $O(n^2)$  cost of computing  $\ell$ , and otherwise set  $n_0 = n$ , so that the whole of the MCMC output was used to select  $\Gamma$ . Python and MATLAB packages are provided and their usage is described in Appendix B.

## 4 Empirical Assessment

The purpose of this section is to compare and contrast the performance of **Stein Thinning** with existing widely-used heuristics for post-processing of MCMC output. In particular, we compare the following methods:

- The standard approach, which identifies a burn-in period  $b$  using either  $\hat{b}^{\text{GR},L}$  or  $\hat{b}^{\text{VK},L}$ , as described in Section 2.1, and combines this with one of the thinning strategies (i), (ii) or (iii) described in Section 2.2 for selection of  $t$ , leading to an index set  $\pi$  of cardinality  $m$ .

- The **Stein Thinning** algorithm that we have proposed, with each of the kernel choices described in Section 3.4.

Our test-bed comprises a set of parameter inference problems arising in ordinary differential equation (ODE) models, including a challenging high-dimensional calcium signalling model that motivated this work. In Section 4.1 we describe the generic structure of a parameter inference problem for an ODE and in Section 4.2 we present typical MCMC methods that might be employed in this context. The 38-dimensional calcium model is presented in detail in Section 4.4, but the challenging nature of the likelihood renders this model unsuitable for conducting a thorough *in silico* assessment, since obtaining repeated instantiations of MCMC is impractical. Therefore in Section 4.3 we first consider a simpler ODE model where it is possible to run many iterations of an MCMC method. In both instances the aim is to post-process the output from MCMC, in order to produce an accurate empirical approximation of the posterior supported on a small number  $m \ll n$  of the states that were visited.

## 4.1 Parameter Inference for ODEs

Consider the solution  $u$  of a system of  $q$  coupled ODEs of the form

$$\begin{aligned} \frac{du_1}{dt} &= f_1(t, u_1, \dots, u_q; x) \\ &\vdots \\ \frac{du_q}{dt} &= f_q(t, u_1, \dots, u_q; x), \end{aligned} \tag{17}$$

together with the initial condition  $u(0) = u^0 \in \mathbb{R}^q$ . The functions  $f_i$  that define the gradient field are assumed to depend on a number  $d$  of parameters, collectively denoted  $x \in \mathbb{R}^d$ , and the  $f_i$  are assumed to be differentiable with respect to  $u_1, \dots, u_q$  and  $x$ . It is assumed that  $u(t)$  exists and is unique on an interval  $t \in [0, T]$  for all values  $x \in \mathbb{R}^d$ . For simplicity in the sequel we assume that the initial condition  $u^0$  is not dependent on  $x$  and is known. The goal is to make inferences about the parameters  $x$  based on noisy observations of the state vector  $u(t_i)$  at discrete times  $t_i$ ; this information is assumed, for simplicity of presentation, to be contained in a likelihood of the form

$$\mathcal{L}(x) := \prod_{i=1}^N \phi_i(u(t_i)) \tag{18}$$

where the functions  $\phi_i : \mathbb{R}^q \rightarrow [0, \infty)$ , describing the nature of the measurement at time  $t_i$ , are to be specified. In this paper we are focussed on Bayesian inference, so that  $x$  is endowed with a prior density  $\pi(x)$  and the posterior of interest  $P$  admits a density  $p(x) \propto \pi(x)\mathcal{L}(x)$ . Computation of the gradient  $\nabla \log p$  therefore requires computation of  $\nabla \log \pi$  and  $\nabla \log \mathcal{L}$ ; the latter can be performed by augmenting the system in (17) with the *sensitivity equations*, as described in Appendix C.

## 4.2 MCMC Methods

To ensure that our empirical findings generalise across a broad spectrum of MCMC algorithms, we implemented four different Metropolis–Hastings samplers that differ according to the sophistication of the proposal. The generic structure of the proposal mechanism is  $x^* = x_{n-1} + H \nabla \log p(x_{n-1}) + G \xi_n$ , where the  $\xi_n \sim \mathcal{N}(0, I)$  are independent and  $H$  and  $G$  are specified in Table 4 of Appendix C for each type of proposal used. The simplest proposals that we considered are the Gaussian random walk (RW) and the adaptive Gaussian random walk (ADA-RW; Haario et al., 1999) proposals, which propose simple moves in random directions from  $x_{n-1}$ , with i.i.d. components in RW and correlated components in ADA-RW. As a canonical example of a more sophisticated proposal, the Metropolis-adjusted Langevin algorithm (MALA; Roberts and Tweedie, 1996) takes a step in the direction of increasing Euclidean gradient, perturbed by Gaussian noise, thus aiming to move faster towards high posterior regions. The different scale of each parameter can be a cause of poor mixing for MALA. This is obviated in the preconditioned version of the algorithm (PRECOND-MALA; Girolami and Calderhead, 2011), which employs a preconditioner based on the Fisher information matrix. Other MCMC algorithms could be considered, but the Metropolis–Hastings algorithms that we considered were selected on the basis that we were able to successfully implement them on the challenging calcium signalling model in Section 4.4, which required manually interfacing with the numerical integrator to produce reliable output.

In the following we report empirical results based on two different systems of ODEs, comparing traditional burn-in and thinning procedures with **Stein Thinning**. First, we consider a synthetic low-dimensional examples ( $d = 4$ ), the Lotka–Volterra model (Section 4.3). We then analyse a challenging real-data example with a high-dimensional parameter ( $d = 38$ ) whose components are strongly correlated (Section 4.4).

## 4.3 Lotka–Volterra

The first example that we consider is the famous predator-prey model of Lotka (1926) and Volterra (1926). This describes the oscillatory evolution of prey ( $u_1$ ) and predator ( $u_2$ ) species in a closed environment. The prey has an intrinsic mechanism for growth proportional to its abundance, described by a parameter  $\theta_1 > 0$ , whilst interaction with the predator leads to a decrease in the prey population at a rate described by a parameter  $\theta_2 > 0$ . Conversely, the predator has an intrinsic mechanism for decline proportional to its abundance, described by a parameter  $\theta_3 > 0$ , whilst interaction with the prey leads to an increase in the predator population at a rate described by a parameter  $\theta_4 > 0$ . The resulting system of ODEs is:

$$\begin{aligned}\frac{du_1}{dt} &= \theta_1 u_1 - \theta_2 u_1 u_2, \\ \frac{du_2}{dt} &= \theta_4 u_1 u_2 - \theta_3 u_2.\end{aligned}$$

To cast this model in the setting of Section 3 we set  $x \in \mathbb{R}^4$  to be the vector whose entries are  $\log(\theta_1), \dots, \log(\theta_4)$ , so that we have a  $d = 4$  dimensional parameter for which inference is performed.

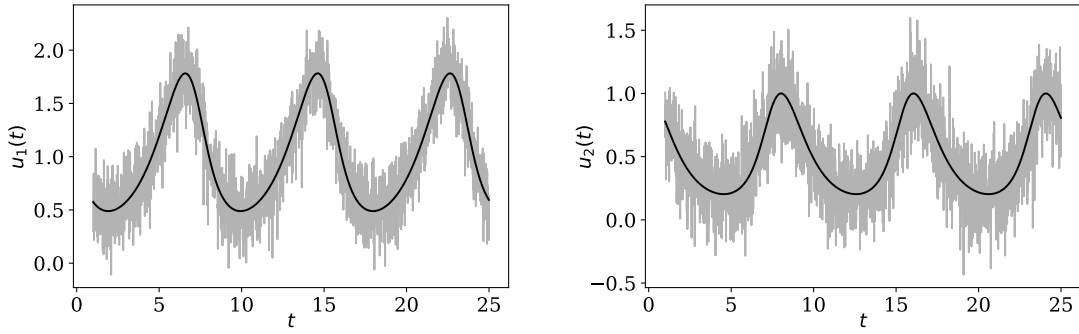


Figure 2: Data (gray) and ODE solution corresponding to the true parameters (black) for the Lotka-Volterra model.

The experiment that we report considers synthetic data which are corrupted by Gaussian noise such that the terms  $\phi_i$  in (18) are equal to

$$\phi_i(u(t_i)) \propto \exp\left(-\frac{1}{2}(y_i - u(t_i))^\top C^{-1}(y_i - u(t_i))\right)$$

with  $C = \text{diag}(0.2^2, 0.2^2)$ . The initial condition was  $u(0) = (1, 1)$  and the data-generating parameters were  $x = \log(\theta)$ , with  $\theta = (0.67, 1.33, 1, 1)$ . The times  $t_i$ ,  $i = 1, \dots, 2400$ , at which data were obtained were taken to be uniformly spaced on  $[0, 25]$ . This relatively high frequency of observation was used to pre-empt a similarly high frequency observation process in the calcium signalling model of Section 4.4. Figure 2 displays the dataset. A standard Gaussian prior  $\pi(x)$  was placed on the parameter  $x$  and each of the MCMC methods in Section 4.2 was applied to approximately sample from the posterior  $P$ .

Trace plots for each MCMC method, of length  $n = 2 \times 10^6$ , are presented in Figure 3. From these it is clear that a burn-in period  $b > 0$  is required, and that  $b$  should depend on the MCMC method used. For each method we therefore computed the (univariate and multivariate) GR and VK diagnostics, to arrive at candidate values  $b$  for the burn-in period. For a full comparison with the literature, we compute convergence diagnostics with  $L = 1$  and  $L = 5$  chains, but our focus is on the VK diagnostic with  $L = 1$ , which provides the fairest comparison with **Stein Thinning** in terms of the samples that are available to the method. The over-dispersed initial states used for the  $L$  chains are reported in Appendix D.1, Table 5, while the multivariate diagnostics, computed every 1000 iterations, are shown in Figure 4 (univariate diagnostics are presented in Appendix D.1, Figure 14). The values of the thresholds  $\delta(L, \alpha, \epsilon)$  are reported in Table 1. For each sampler, the burn-in period  $b$ , estimated with the scalar convergence diagnostics, are presented in Table 2, where we report the largest value obtained over the set of parameters as overall burn-in period. The convergence diagnostics estimated with the multivariate set of parameters are reported in Table 3. As a conservative choice, for each sampler we select as final burn-in the largest of the burn-in periods produced by the VK diagnostic with one chain only ( $L = 1$ ). From these displays we observe that the GR diagnostic rarely goes below the threshold in the

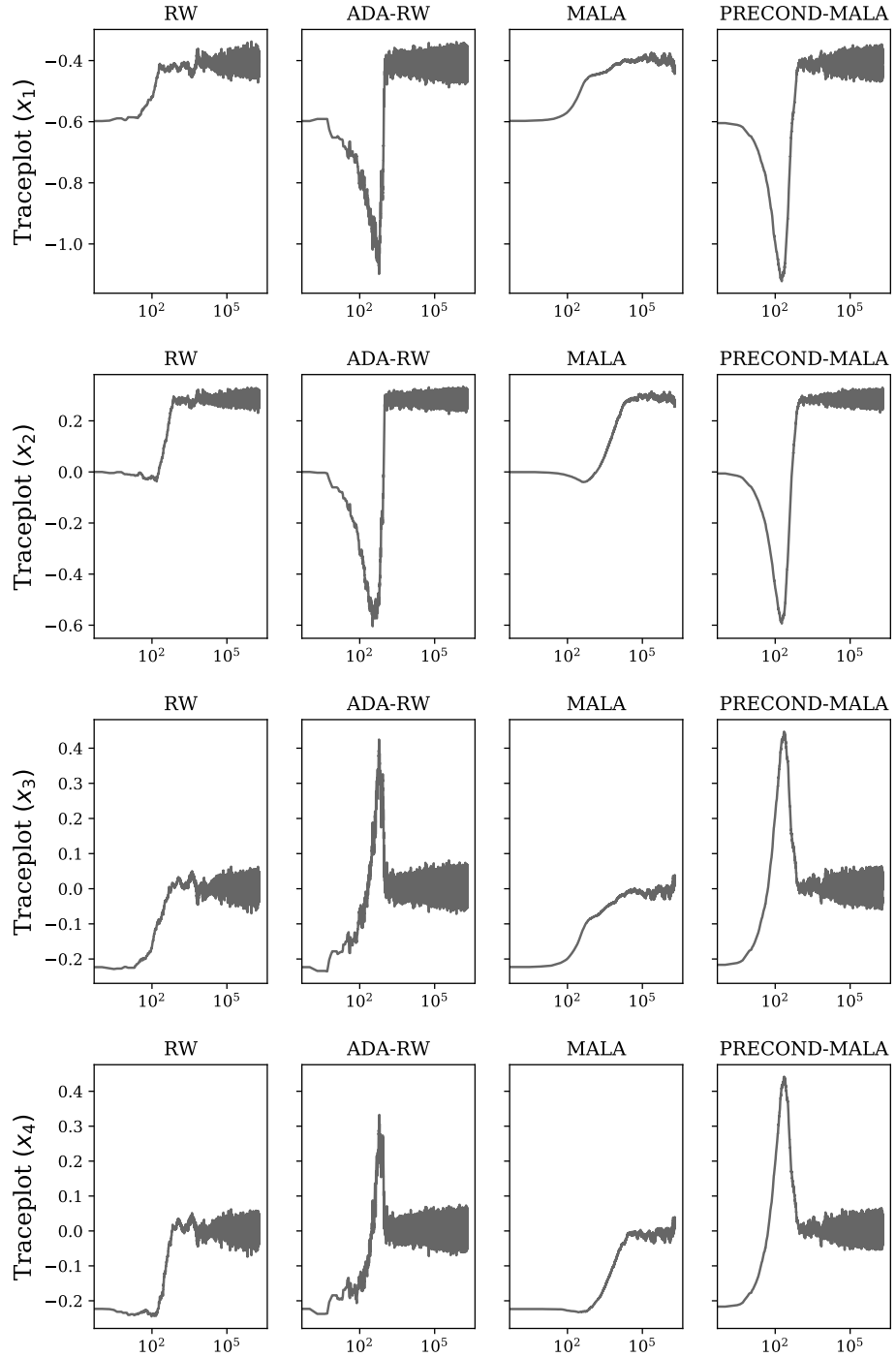


Figure 3: Trace plots for the parameters  $x_i$  in the Lotka-Volterra model, plotted against the MCMC iteration number. Each row corresponds to one of the four parameters, while each column corresponds to one of the four MCMC methods considered.

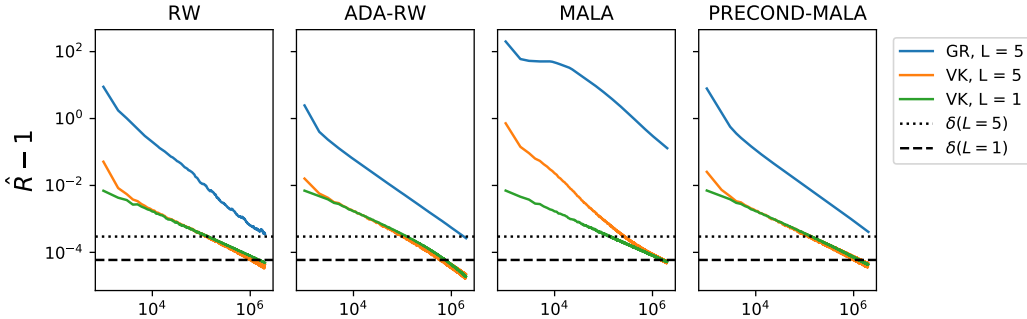


Figure 4: Multivariate convergence diagnostics for Lotka-Volterra, plotted against the MCMC iteration number. The blue line is the GR diagnostic (based on  $L = 5$  chains), while the orange and green lines are the VK diagnostic (based on  $L = 5$  and  $L = 1$  chains, respectively). The dotted ( $L = 5$ ) and dashed ( $L = 1$ ) horizontal lines correspond to the critical values  $\delta(L, \alpha, \epsilon)$ , used to determine the burn-in period; see Table 1.

	Univariate Diagnostics	Multivariate Diagnostics
$L = 5$	$4.07 \times 10^{-4}$	$2.96 \times 10^{-4}$
$L = 1$	$8.13 \times 10^{-5}$	$5.93 \times 10^{-5}$

Table 1: Values of the threshold  $\delta(L, \alpha, \epsilon)$ , with  $\alpha = 0.05$ ,  $\epsilon = 0.05$ , when changing  $L$ , and considering the univariate and multivariate convergence diagnostics  $\hat{R}^{\text{VK},L}$ .

Univariate Diagnostics	$\hat{b}^{\text{GR},5}$	$\hat{b}^{\text{VK},5}$	$\hat{b}^{\text{VK},1}$
RW	$> n$	88,000	954,000
ADA-RW	$> n$	16,000	83,000
MALA	$> n$	424,000	995,000
PRECOND-MALA	$> n$	90,000	820,000

Table 2: Estimated burn-in period for the MCMC output in the Lotka-Volterra model, determined by the scalar GR diagnostic with  $L = 5$  chains,  $\hat{b}^{\text{GR},5}$ , and by the scalar VK diagnostic, with  $L = 5$  and  $L = 1$  chains, respectively  $\hat{b}^{\text{VK},5}$  and  $\hat{b}^{\text{VK},1}$ . The symbol “ $> n$ ” indicates the case in which a diagnostic did not go below the critical value  $1 + \delta$ .

allowed number of iterations, which is consistent with the empirical observations of Vats and Knudson (2018). Indeed, most convergence diagnostics require that at least half of the MCMC output is discarded. Although well-suited for their intended task of minimising bias in MCMC output, the relatively small number of states left after burn-in removal using a convergence diagnostic is likely to lead to inefficient approximation of  $P$  and derived quantities of interest. The use of an optimality criterion enables **Stein Thinning** to directly address this bias-variance trade-off.

Having identified a burn-in period, we thinned the remainder of the sample path according to one of the three strategies presented in Section 2.2. The resulting index sets  $\pi$  are displayed, for  $m = 4$ , in Figure 5, based on output from the RW MCMC method. These

Multivariate Diagnostics	$\hat{b}^{\text{GR},5}$	$\hat{b}^{\text{VK},5}$	$\hat{b}^{\text{VK},1}$
RW	$> n$	119,00	1,512,000
ADA-RW	1,797,000	99,000	123,000
MALA	$> n$	259,000	1,573,000
PRECOND-MALA	$> n$	114,000	1,251,000

Table 3: Estimated burn-in iterations for the MCMC output for the Lotka-Volterra model, determined by the multivariate Gelman-Rubin diagnostic with  $L = 5$  chains,  $\hat{b}^{\text{GR},5}$ , and by the multivariate Vats-Knudson diagnostic, with  $L = 5$  and  $L = 1$  chains, respectively  $\hat{b}^{\text{VK},5}$  and  $\hat{b}^{\text{VK},1}$ . The symbol “ $> n$ ” indicates the case in which a diagnostic did not go below the critical value  $1 + \delta$ .

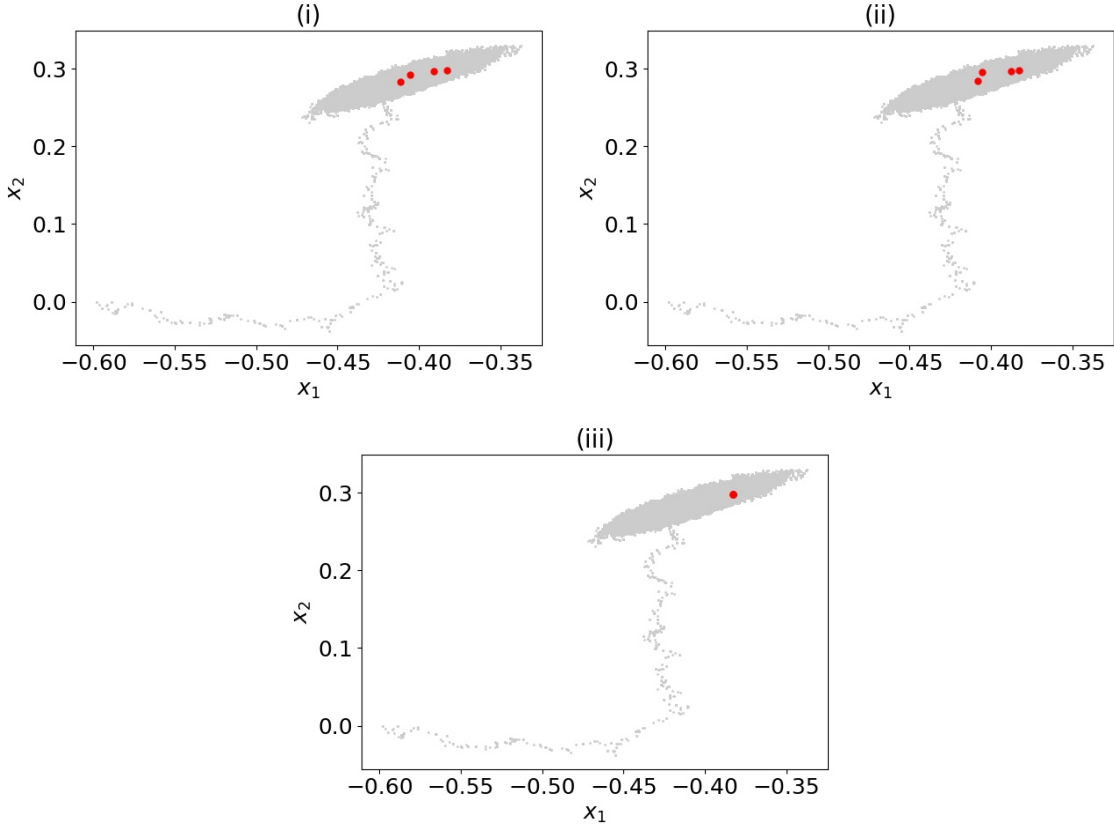


Figure 5: Projections on the first two coordinates of the RW MCMC output for the Lotka-Volterra model, together with the first  $m = 4$  points obtained through traditional burn-in and thinning strategies (i)-(iii).

should be compared to sets of the same cardinality produced by **Stein Thinning** applied to the same MCMC sample path, shown in Figure 6. From these figures, it is apparent that benchmark methods (i)-(iii) suffer from a combination of (a) sub-optimal selection of states, and (b) insufficient diversity in the remainder of the sample path after the burn-in period is removed. Issue (a) is directly addressed through the use of an optimality criterion in

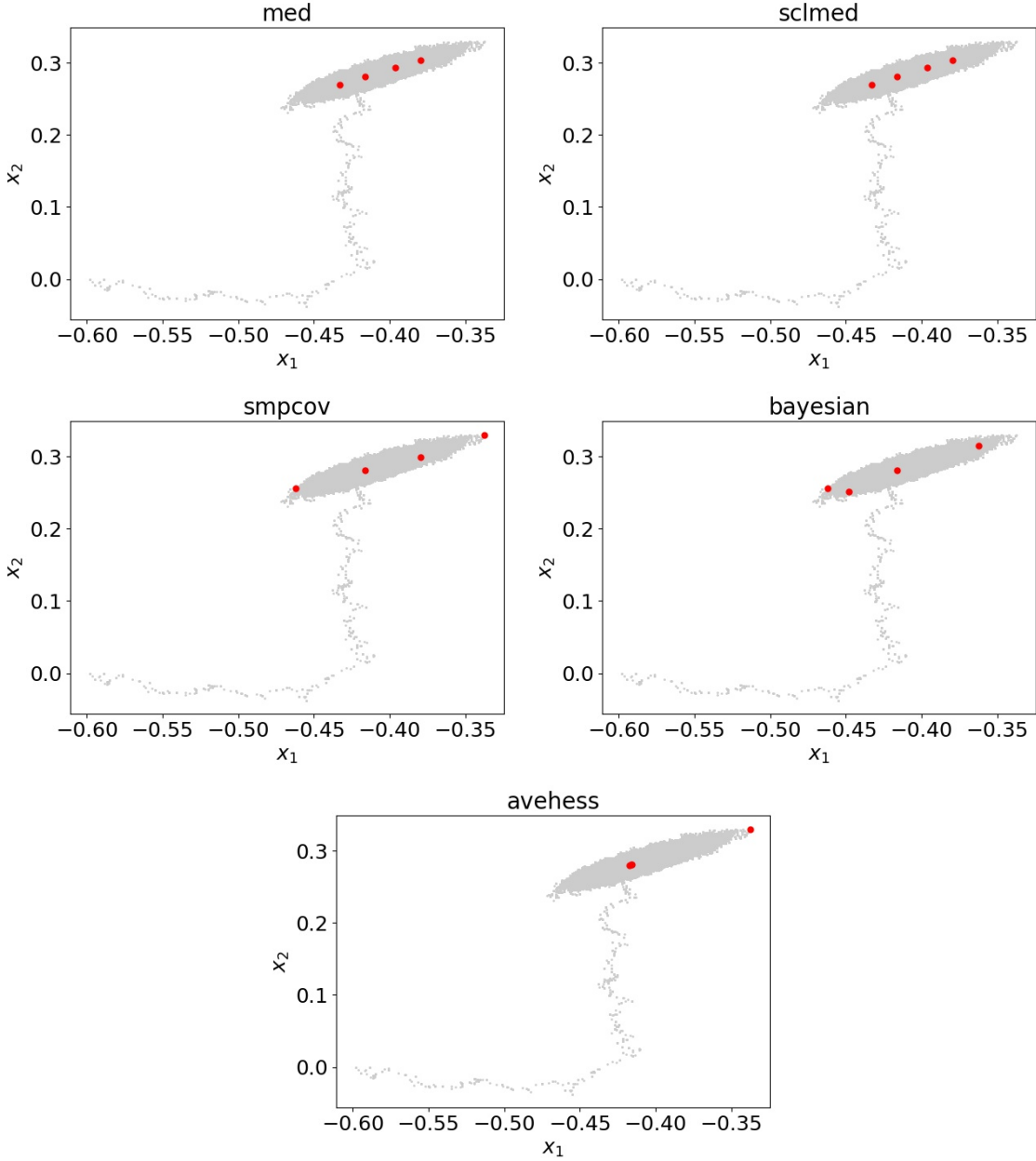


Figure 6: Projections on the first two coordinates of the RW MCMC output for the Lotka-Volterra model, together with the first  $m = 4$  points selected by **Stein Thinning**, for each of the heuristics **med**, **sclmed**, **smpcov**, **bayesian**, **avehess** used to select  $\Gamma$ .

**Stein Thinning**, which typically selects states that are well-separated. Here we note that the **med** and **sclmed** heuristics appear to produce quite reasonable and symmetric point sets, whilst the **smpcov**, **bayesian** and in particular the **avehess** heuristic appear less suitable for use in **Stein Thinning**, at least according to Figure 6. Issue (b) has led to close or identical

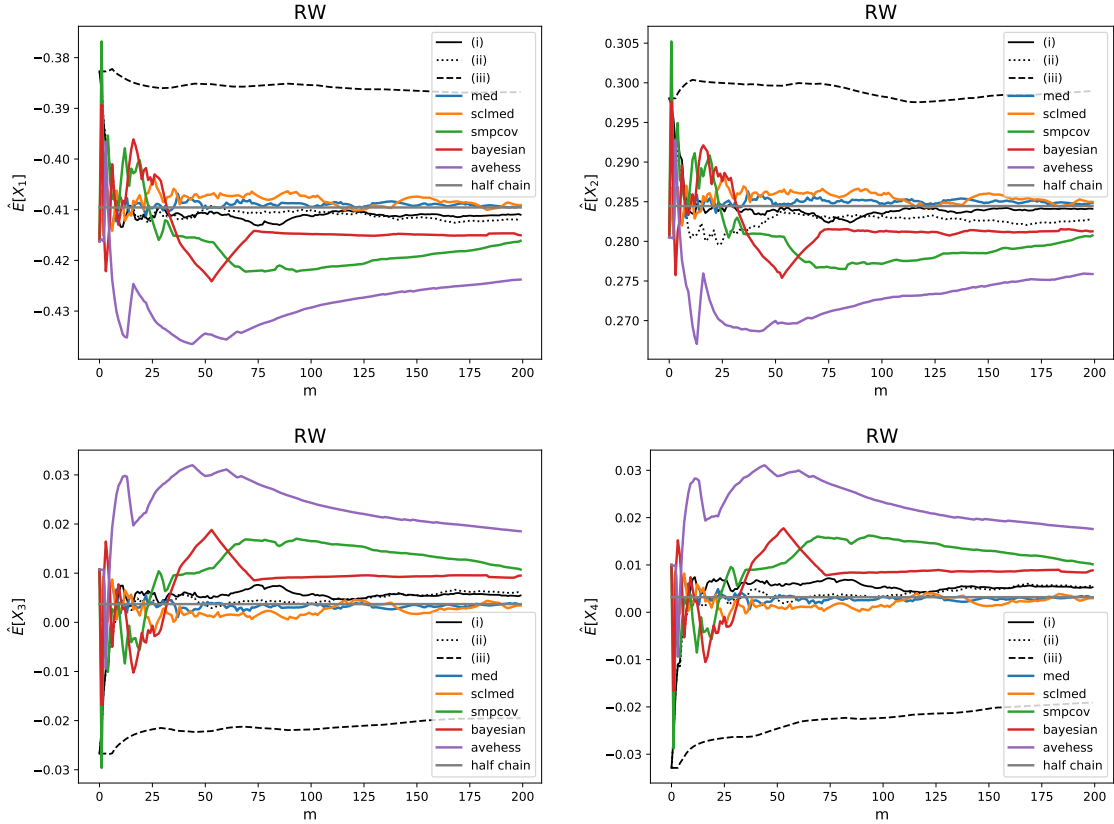


Figure 7: Estimates of the means of the parameters in the Lotka-Volterra model, based on RW MCMC output. The estimators are of the form (3), where  $\pi$  is a set of cardinality  $m$  determined either through traditional burn-in and thinning (black lines) or Stein Thinning (coloured lines). The gray horizontal line is considered to be a ground truth, based on the second half ( $10^6$  states) from the MCMC output.

points being selected when the remainder of the sample path is thinned. Of course, one can in principle run more iterations of MCMC to provide more diversity in the remainder of the sample path after burn-in is removed, but in applications such as the calcium model of Section 4.4 the computational cost associated with each iteration precludes easily obtaining more iterations of an MCMC method. Effective methods to post-process limited output (or, equivalently, a long output from a poorly mixing Markov chain) are therefore practically important.

The apparent improvement at the level of the point set generated from **Stein Thinning**, at least when the `med` or `sclmed` heuristics are used, translates into more accurate approximation of posterior expectations when the cardinality  $m$  is fixed. In Figure 7, we plot approximations of the form (3) for first moments  $f(x) = x_i$ ,  $i = 1, \dots, 4$ , based on RW MCMC, where the negligible cost of evaluating  $f$  in this toy model allows us to produce a ground truth based on the second half ( $n = 10^6$  states) of the MCMC output. From these

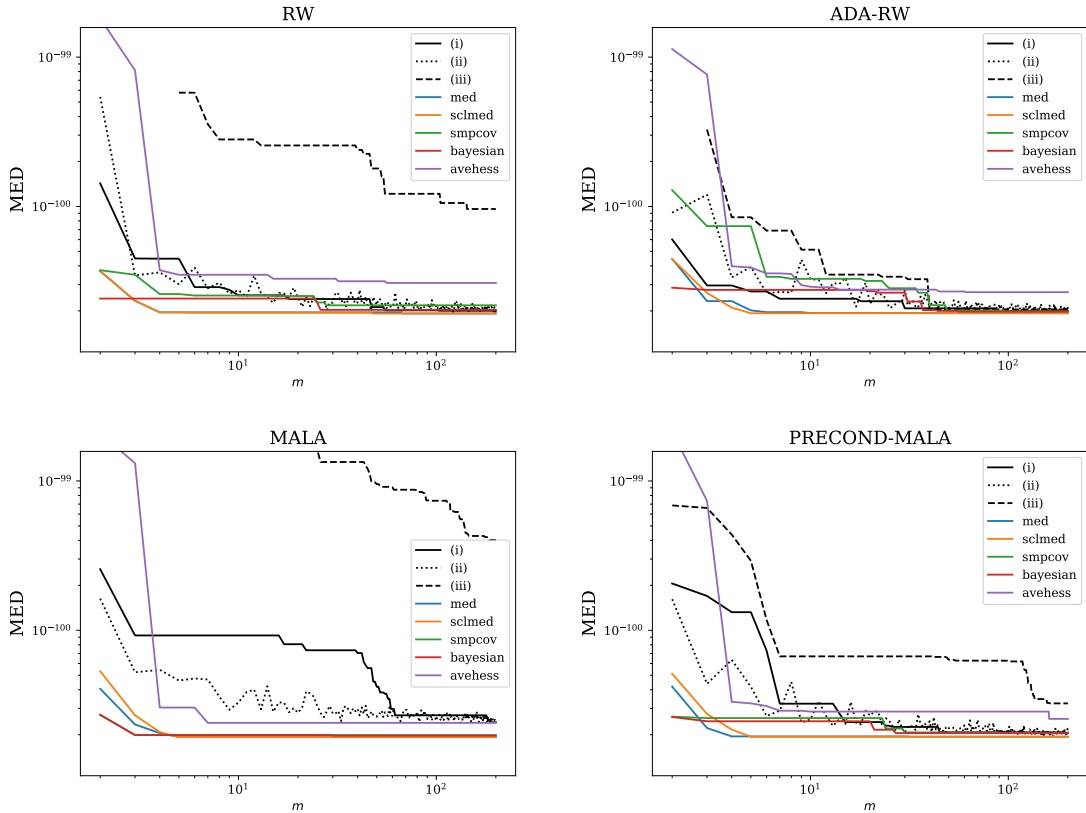


Figure 8: Lotka-Volterra model. Minimum energy design (MED) “distance” to the posterior, for empirical distributions obtained through traditional burn-in and thinning (black lines) and through Stein Thinning (colored lines).

results is apparent that Stein Thinning with `med` and `sclmed` out-performs the alternatives considered. The heuristics `smpcov`, `bayesian` and `avehess` perform poorly, which we interpret as being due to poor estimation of a suitable  $\Gamma$  based on the MCMC output.

To facilitate a more principled assessment than simply visual inspection of first moments, we computed two quantitative measures for how well the resulting empirical distributions approximate the posterior. These were (a) the minimum energy design (MED) “distance” of Joseph et al. (2019), shown in Figure 8, and (b) the KSD with fixed  $\Gamma = 0.000128^{-2}I$ , shown in Figure 9. MED serves as an objective performance measure, while KSD is the performance measure that is being directly optimised in Stein Thinning (albeit with a different  $\Gamma$ ). Our decision to include KSD in the assessment is motivated by two factors; firstly, MED is somewhat insensitive to fine detail, and secondly, Stein discrepancies are the only computable performance measures in the Bayesian context, to the best of our knowledge, that have been proven to provide convergence control.

Figure 8 indicates that, of the strategies presented in Section 2.2, strategy (ii) performs best across all four Markov chains and across a broad range of  $m$  from 1 to 200. Despite this,

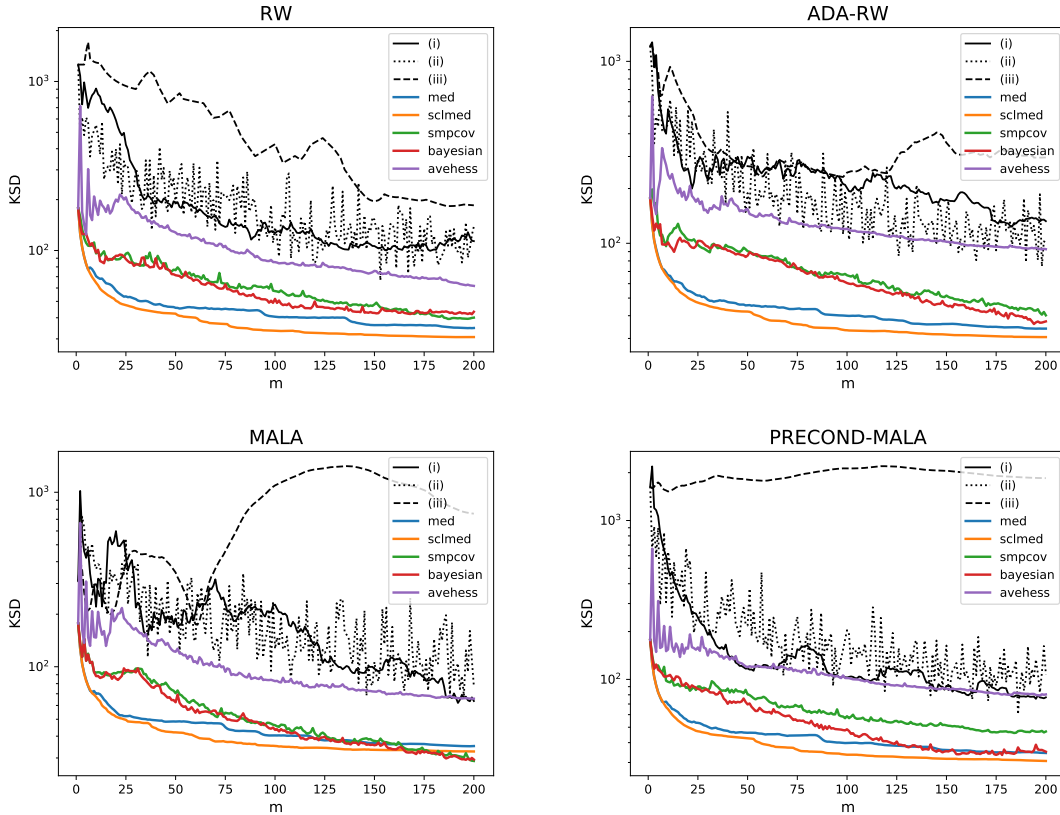


Figure 9: Lotka-Volterra model. Kernel Stein discrepancy (KSD) from the posterior, for empirical distributions obtained through traditional burn-in and thinning (black lines) and through Stein Thinning (colored lines), for each of the MCMC methods RW, ADA-RW, MALA and PRECOND-MALA.

all of the instances of Stein Thinning that we considered performed at least as well as (ii), and the variants that used either the `med` heuristic or the `sclmed` heuristic performed better than every other method considered. The KSD measure used in Figure 9 exaggerates the improvement of Stein Thinning over standard methods, but the performance ordering of the methods is the same as that when assessed using MED. Note that the actual values taken by MED and KSD are difficult to interpret, owing to their somewhat indirect construction that is required to avoid computation of the normalisation constant. Note also that neither MED or KSD values will tend to 0 as  $m \rightarrow \infty$  in this experiment, since the number  $n$  of MCMC iterations was fixed.

#### 4.4 Calcium Signalling Model

Our final and motivating example is a calcium signalling model, shown in Figure 10. Recall that with each beat an electrical wave propagates across the heart, electrically activating the muscle cells. This initiates an intracellular calcium signal that activates the sub-cellular

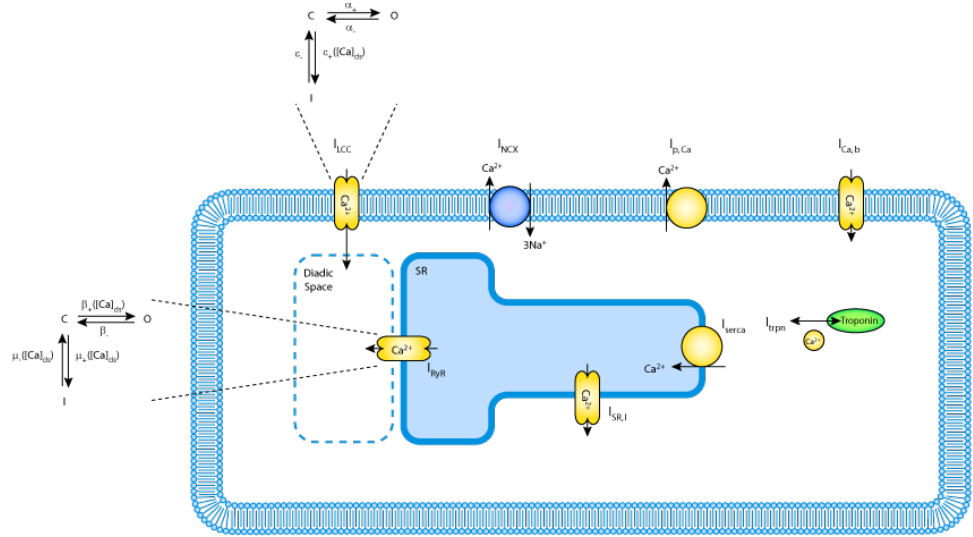


Figure 10: Calcium signalling model; a schematic representation due to Hinch et al. (2004). The model consists of 6 coupled ordinary differential equations and depends upon 38 real-valued parameters that must be estimated from an experimental dataset.

sarcomere, causing the muscle cell to contract and the heart to beat. The intracellular calcium signal is crucial for healthy cardiac function. However, under pathological conditions, dysregulation of this intra-cellular signal can play a central role in the initiation and sustenance of life-threatening arrhythmias. Computational models are increasingly being applied to study this highly-orchestrated multi-scale signalling cascade to determine how changes in cell-scale calcium regulation, encoded in calcium model parameters, impact whole-organ cardiac function (Campos et al., 2015; Niederer et al., 2019; Colman, 2019). The computational cost of simulating from tissue-scale and organ-scale models is high, with single simulations taking thousands of CPU hours (Niederer et al., 2011; Augustin et al., 2016; Strocchi et al., 2020). This limits the capacity to propagate uncertainty in calcium signalling model parameters up to organ-scale simulations, so that at present it remains unclear how uncertainty in calcium signalling parameters impacts the predictions made by a whole-organ model. Our motivation for developing **Stein Thinning** was to obtain a compressed representation of the posterior distribution for the parameters  $\theta \in \mathbb{R}^{38}$ , based on a cell-scale experimental dataset, which can subsequently be propagated through a whole-organ model.

This motivating problems entails a second complication in that, compared to the example in Section 4.3, the development of an efficient MCMC method appears to be difficult. The posterior distribution, which is defined below, exhibits strong and nonlinear dependencies among the parameters such that the posterior is effectively supported on a sub-manifold of  $\mathbb{R}^{38}$ . MCMC methods that exploit first order gradient information (only) can perform worse than gradient-free MCMC methods in these situations (Livingstone and Zanella, 2019), since a move in the direction of increasing gradient corresponds to a step perpendicular to the sub-

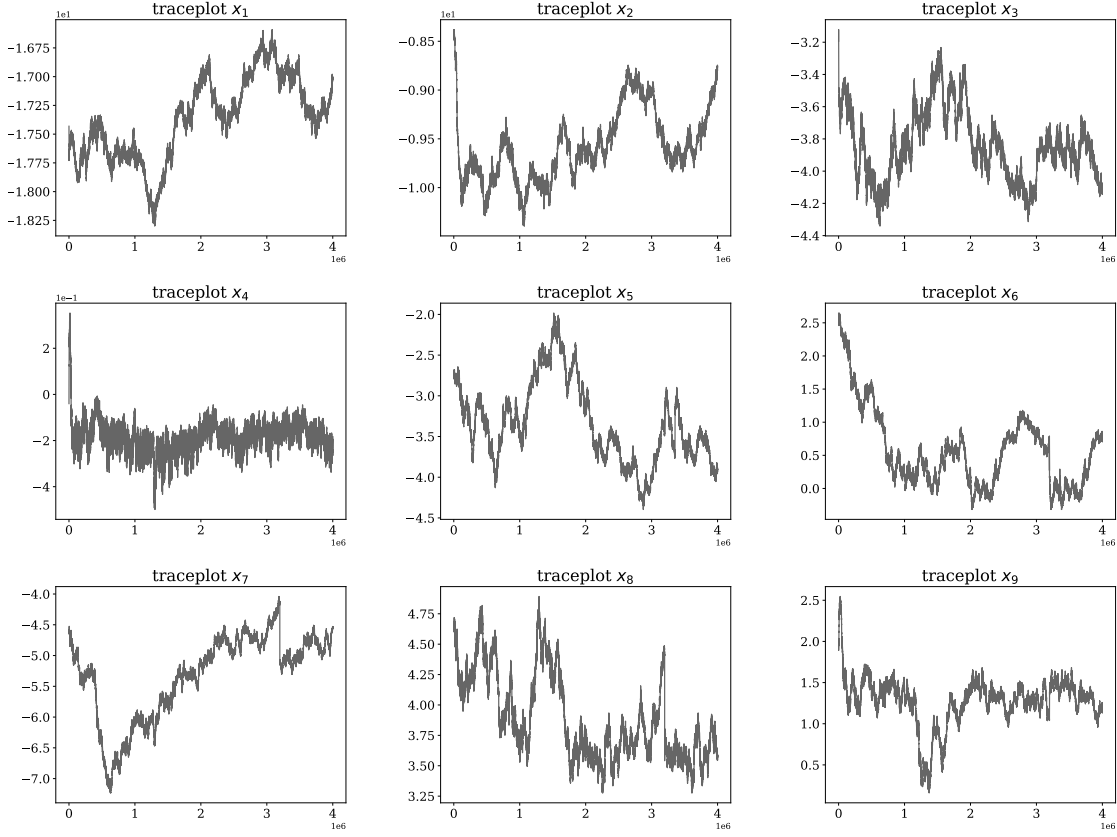


Figure 11: Trace plots for the first 9 (of 38) parameters  $x_i$  in the cardiac signalling model, plotted against the MCMC iteration number. Each panel corresponds to one parameter.

manifold, such that the probability of actually landing on the sub-manifold is small. Thus in the experiment that follows we do not expect the full MCMC output to provide an accurate approximation of the posterior, and the potential for **Stein Thinning** to perform some bias correction will be explored (in a similar manner to Liu and Lee, 2017; Hodgkinson et al., 2020).

The calcium signalling model in Figure 10 is represented by a coupled system of  $q = 6$  ODEs and depends on  $d = 38$  real-valued parameters, which are to be estimated based on an experimental dataset. The data consist of measurements of calcium concentration in the cytoplasm whilst the cell was externally stimulated, so that only one of the state variables,  $u_5$ , was observed. Our likelihood took the simple Gaussian form  $\phi_i(u(t_i)) \propto \exp(-\frac{1}{2\sigma^2}(y_i - u_5(t_i))^2)$  with  $\sigma = 2.07 \times 10^{-8}$ . The ODE was numerically solved using CVODES (Hindmarsh et al., 2005) and sensitivities were computed by solving the forward sensitivity equations; see Appendix C. Further details of the calcium model are provided in Appendix D.2, but such is the complexity of the model, the expert elicited prior, the data pre-processing procedure and numerical details associated with the ODE solver, that we reserve full details for a sequel, in preparation as of May 17, 2022. Full details are available

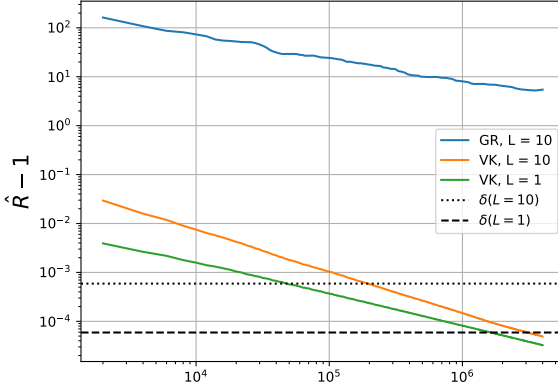


Figure 12: Multivariate convergence diagnostics for the calcium signalling model, plotted against the MCMC iteration number. The blue line is the GR diagnostic (based on  $L = 10$  chains), while the orange and green lines are the VK diagnostic (based on  $L = 10$  and  $L = 1$  chains, respectively). The dotted ( $L = 10$ ) and dashed ( $L = 1$ ) horizontal lines correspond to the critical values  $\delta(L, \alpha, \epsilon)$ , equal to  $5.91 \times 10^{-4}$  and  $5.91 \times 10^{-5}$ , respectively, used to determine the burn-in period.

on request.

Here we report results for RW MCMC and compare the traditional approach of burn-in removal and thinning to **Stein Thinning**. Trace plots are shown in Figure 11 and indicate poor mixing of the MCMC method, which is expected given the challenging nature of this task. The multivariate convergence diagnostics are presented in Figure 12. As before, the GR diagnostic does not converge in the allowed computation time, while the burn-in estimates obtained using the VK diagnostic are  $\hat{b}^{\text{VK},10} = 192,000$  and  $\hat{b}^{\text{VK},1} = 1,626,000$ . In order to simulate a fixed CPU time (of the order of magnitude of a few days), we consider the burn-in time  $\hat{b}^{\text{VK},10}$ , and restrict the MCMC output to the first  $n = 1,250,000$  iterations only. Figure 13 reports the KSD with  $\Gamma = 4^{-2}I$ , for index sets of cardinality up to  $m = 200$ . These results show that **Stein Thinning** with any choice of pre-conditioner outperforms the benchmark strategies on this challenging task, and that overall the **med** and **sclmed** heuristics performed best. Closer investigation of the selected point sets reveals that these two heuristics contain many duplicates of a small number of points, essentially forming a weighted empirical measure on those points. This suggests that the MCMC output is not representative of the posterior  $P$  and that only the “nearest” points to  $P$  are being selected. This further suggests that **Stein Thinning** is able, to some extent, to provide a correction for poorly mixing Markov chains, whilst also facilitating compression of the MCMC output.

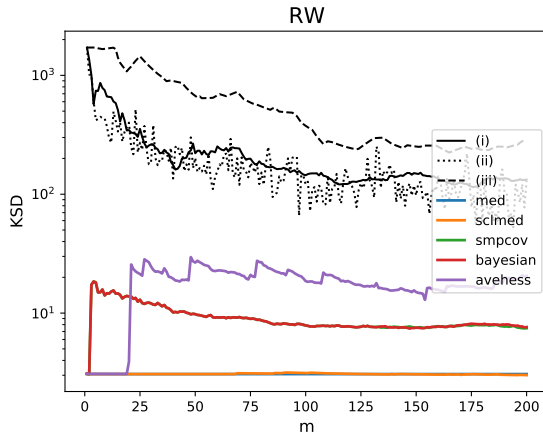


Figure 13: Calcium signalling model. Kernel Stein discrepancy (KSD) from the posterior, for empirical distributions obtained through traditional burn-in and thinning (black lines) and through **Stein Thinning** (colored lines), for the RW MCMC method.

## 5 Conclusion

In this paper, standard approaches used to post-process and compress output from MCMC, based on removal of the burn-in period and thinning of the remainder, were identified as being sub-optimal when one considers the approximation quality of the empirical distribution that is obtained. A novel method, **Stein Thinning**, was proposed that seeks a subset of the MCMC output, of fixed cardinality, such that the associated empirical approximation is close to optimal. To the best of our knowledge, the theoretical analysis that we have provided for **Stein Thinning** is the first to handle the effect of the post-processing procedure jointly with the randomness involved in simulating from the Markov chain, such that consistency of the overall estimator is established.

Although we focussed on MCMC, the proposed method can be applied to any computational method that provides a collection of states as output. These include approximate (biased) MCMC methods such as those described in Alquier et al. (2016), where **Stein Thinning** may be able to provide bias correction (under similar conditions as those considered in Hodgkinson et al., 2020).

Our research was motivated by challenging parameter inference problems that arise in ODEs, in particular in cardiac modelling where one is interested in propagating calcium signalling parameter uncertainty through expensive whole heart simulations – a task that would naïvely be impractical or impossible using standard MCMC output. Our future research will exploit **Stein Thinning** in this context and will enable us to perform scientific investigation of the impact of calcium parameter uncertainty on whole heart simulations that were not possible beforehand.

**Acknowledgements** The authors are grateful for support from the Lloyd’s Register Foundation programme on data-centric engineering and the programme on health and medical sciences at the Alan Turing Institute. MR, SN and CJO were supported by the British Heart Foundation (BHF; SP/18/6/33805). JC was supported by the UKRI Strategic Priorities Fund (EP/T001569/1). PS was supported by the BHF (RG/15/9/31534). SN was supported by the EPSRC (EP/P01268X/1, NS/A000049/1, EP/M012492/1), the BHF (PG/15/91/31812, FS/18/27/33543), the NIHR (II-LB-1116-20001) and the Wellcome Trust (WT 203148/Z/16/Z). The authors thank Matthew Graham for insight into the failure of gradient-based MCMC on the calcium signalling model.

## References

P. Alquier, N. Friel, R. Everitt, and A. Boland. Noisy Monte Carlo: Convergence of Markov chains with approximate transition kernels. *Statistics and Computing*, 26(1-2):29–47, 2016.

Y. F. Atchadé et al. Markov chain Monte Carlo confidence intervals. *Bernoulli*, 22(3):1808–1838, 2016.

C. M. Augustin, A. Neic, M. Liebmann, A. J. Prassl, S. A. Niederer, G. Haase, and G. Plank. Anatomically accurate high resolution modeling of human whole heart electromechanics: a strongly scalable algebraic multigrid solver method for nonlinear deformation. *Journal of Computational Physics*, 305:622–646, 2016.

F. Bach, S. Lacoste-Julien, and G. Obozinski. On the equivalence between herding and conditional gradient algorithms. In *Proceedings of the International Conference on Machine Learning*, pages 1355–1362, 2012.

A. Barp, C. Oates, E. Porcu, and M. Girolami. A Riemannian-Stein kernel method. *arXiv:1810.04946*, 2018.

A. Berlinet and C. Thomas-Agnan. *Reproducing Kernel Hilbert Spaces in Probability and Statistics*. Springer Science & Business Media, New York, 2004.

S. P. Brooks and A. Gelman. General methods for monitoring convergence of iterative simulations. *Journal of Computational and Graphical Statistics*, 7(4):434–455, 1998.

F. O. Campos, Y. Shiferaw, A. J. Prassl, P. M. Boyle, E. J. Vigmond, and G. Plank. Stochastic spontaneous calcium release events trigger premature ventricular complexes by overcoming electrotonic load. *Cardiovascular Research*, 107(1):175–183, 2015.

B. Carpenter, A. Gelman, M. D. Hoffman, D. Lee, B. Goodrich, M. Betancourt, M. Brubaker, J. Guo, P. Li, and A. Riddell. Stan: A probabilistic programming language. *Journal of Statistical Software*, 76(1), 2017.

W. Y. Chen, L. Mackey, J. Gorham, F.-X. Briol, and C. J. Oates. Stein points. In *Proceedings of the 35th International Conference on Machine Learning*, 2018.

W. Y. Chen, A. Barp, F.-X. Briol, J. Gorham, L. Mackey, M. Girolami, and C. J. Oates. Stein points Markov chain Monte Carlo. In *Proceedings of the 36th International Conference on Machine Learning*, 2019.

K. Chwialkowski, H. Strathmann, and A. Gretton. A kernel test of goodness of fit. In *Proceedings of the 33rd International Conference on Machine Learning*, 2016.

M. A. Colman. Arrhythmia mechanisms and spontaneous calcium release: Bi-directional coupling between re-entrant and focal excitation. *PLoS Computational Biology*, 15(8), 2019.

M. K. Cowles and B. P. Carlin. Markov chain Monte Carlo convergence diagnostics: a comparative review. *Journal of the American Statistical Association*, 91(434):883–904, 1996.

A. Duncan, N. Nüsken, and L. Szpruch. On the geometry of Stein variational gradient descent. *arXiv:1912.00894*, 2019.

R. Dwivedi, O. N. Feldheim, O. Gurel-Gurevich, and A. Ramdas. The power of online thinning in reducing discrepancy. *Probability Theory and Related Fields*, 174(1-2):103–131, 2019.

J. M. Flegal, M. Haran, and G. L. Jones. Markov chain Monte Carlo: Can we trust the third significant figure? *Statistical Science*, 23(2):250–260, 2008.

D. Garreau, W. Jitkrittum, and M. Kanagawa. Large sample analysis of the median heuristic. *arXiv:1707.07269*, 2018.

A. E. Gelfand and A. F. Smith. Sampling-based approaches to calculating marginal densities. *Journal of the American Statistical Association*, 85(410):398–409, 1990.

A. Gelman and D. B. Rubin. Inference from iterative simulation using multiple sequences. *Statistical science*, 7(4):457–472, 1992.

A. Gelman, J. B. Carlin, H. S. Stern, D. B. Dunson, A. Vehtari, and D. B. Rubin. *Bayesian Data Analysis*, volume 2. CRC press, 2014.

S. Geman and D. Geman. Stochastic relaxation, Gibbs distributions, and the Bayesian restoration of images. *IEEE Transactions on Pattern Analysis and Machine Intelligence*, (6):721–741, 1984.

C. J. Geyer. Practical Markov chain Monte Carlo. *Statistical Science*, 7(4):473–483, 1992.

M. Girolami and B. Calderhead. Riemann manifold Langevin and Hamiltonian Monte Carlo methods. *Journal of the Royal Statistical Society, Series B*, 73(2):123–214, 2011.

J. Gorham and L. Mackey. Measuring sample quality with Stein’s method. In *Proceedings of the 29th Conference on Neural Information Processing Systems*, 2015.

J. Gorham and L. Mackey. Measuring sample quality with kernels. In *Proceedings of the 34th International Conference on Machine Learning*, 2017.

P. J. Green, K. Latuszyński, M. Pereyra, and C. P. Robert. Bayesian computation: a summary of the current state, and samples backwards and forwards. *Statistics and Computing*, 25(4):835–862, 2015.

A. Gretton, K. M. Borgwardt, M. J. Rasch, B. Schölkopf, and A. J. Smola. A kernel method for the two-sample-problem. In *Proceedings of the 20th Conference on Neural Information Processing Systems*, 2006.

H. Haario, E. Saksman, and J. Tamminen. Adaptive proposal distribution for random walk Metropolis algorithm. *Computational Statistics*, 14(3):375–396, 1999.

W. K. Hastings. Monte Carlo sampling methods using Markov chains and their applications. 1970.

R. Hinch, J. Greenstein, A. Tanskanen, L. Xu, and R. Winslow. A simplified local control model of calcium-induced calcium release in cardiac ventricular myocytes. *Biophysical Journal*, 87(6):3723–3736, 2004.

A. C. Hindmarsh, P. N. Brown, K. E. Grant, S. L. Lee, R. Serban, D. E. Shumaker, and C. S. Woodward. SUNDIALS: Suite of nonlinear and differential/algebraic equation solvers. *ACM Transactions on Mathematical Software (TOMS)*, 31(3):363–396, 2005.

L. Hodgkinson, R. Salomone, and F. Roosta. The reproducing Stein kernel approach for post-hoc corrected sampling. *arXiv:2001.09266*, 2020.

J. Huggins and L. Mackey. Random feature Stein discrepancies. In *Proceedings of the 31st Conference on Neural Information Processing Systems*, 2018.

G. L. Jones and J. P. Hobert. Honest exploration of intractable probability distributions via Markov chain Monte Carlo. *Statistical Science*, 16(4):312–334, 2001.

V. R. Joseph, T. Dasgupta, R. Tuo, and C. Wu. Sequential exploration of complex surfaces using minimum energy designs. *Technometrics*, 57(1):64–74, 2015.

V. R. Joseph, D. Wang, L. Gu, S. Lyu, and R. Tuo. Deterministic sampling of expensive posteriors using minimum energy designs. *Technometrics*, 61(3):297–308, 2019. To appear.

C. Knudson and D. Vats. *stableGR*, 2020. R package version 1.0.

H. Le, A. Lewis, K. Bharath, and C. Fallaize. A diffusion approach to Stein’s method on Riemannian manifolds. *arXiv:2003.11497*, 2020.

C. Liu and J. Zhu. Riemannian Stein variational gradient descent for Bayesian inference. In *Proceedings of the 32nd AAAI Conference on Artificial Intelligence*, 2018.

Q. Liu. Stein variational gradient descent as gradient flow. In *Proceedings of the 31st Conference on Neural Information Processing Systems*, 2017.

Q. Liu and J. D. Lee. Black-box importance sampling. In *Proceedings of the 20th International Conference on Artificial Intelligence and Statistics*, 2017.

Q. Liu and D. Wang. Stein variational gradient descent: A general purpose Bayesian inference algorithm. In *Proceedings of the 30th Conference on Neural Information Processing Systems*, 2016.

Q. Liu, J. D. Lee, and M. I. Jordan. A kernelized Stein discrepancy for goodness-of-fit tests and model evaluation. In *Proceedings of the 33rd International Conference on Machine Learning*, 2016.

S. Livingstone and G. Zanella. On the robustness of gradient-based MCMC algorithms. *arXiv:1908.11812*, 2019.

A. J. Lotka. Elements of physical biology. *Science Progress in the Twentieth Century (1919-1933)*, 21(82):341–343, 1926.

D. J. Lunn, A. Thomas, N. Best, and D. Spiegelhalter. WinBUGS - a Bayesian modelling framework: concepts, structure, and extensibility. *Statistics and Computing*, 10(4):325–337, 2000.

S. Mak and V. R. Joseph. Support points. *The Annals of Statistics*, 46(6A):2562–2592, 2018.

S. Meyn and R. Tweedie. *Markov Chains and Stochastic Stability*. Springer Science & Business Media., 2012.

S. P. Meyn and R. L. Tweedie. Computable bounds for geometric convergence rates of Markov chains. *The Annals of Applied Probability*, 4(4):981–1011, 1994.

A. Muller. Integral probability metrics and their generating classes of functions. *Advances in Applied Probability*, 29(2):429–443, 1997.

S. Niederer, L. Mitchell, N. Smith, and G. Plank. Simulating human cardiac electrophysiology on clinical time-scales. *Frontiers in Physiology*, 2:14, 2011.

S. A. Niederer, J. Lumens, and N. A. Trayanova. Computational models in cardiology. *Nature Reviews Cardiology*, 16(2):100–111, 2019.

C. J. Oates, M. Girolami, and N. Chopin. Control functionals for Monte Carlo integration. *Journal of the Royal Statistical Society, Series B*, 79(3):695–718, 2017.

A. B. Owen. Statistically efficient thinning of a Markov chain sampler. *Journal of Computational and Graphical Statistics*, 26(3):738–744, 2017.

M. Plummer. JAGS: A program for analysis of Bayesian graphical models using Gibbs sampling. In *Proceedings of the 3rd International Workshop on Distributed Statistical Computing*, 2003.

M. Plummer, N. Best, K. Cowles, and K. Vines. CODA: Convergence diagnosis and output analysis for MCMC. *R News*, 6(1):7–11, 2006. URL <https://journal.r-project.org/archive/>.

R Core Team. *R: A Language and Environment for Statistical Computing*. R Foundation for Statistical Computing, 2020. URL <https://www.R-project.org>.

C. Robert and G. Casella. *Monte Carlo Statistical Methods*. Springer Science & Business Media, 2013.

G. O. Roberts and J. S. Rosenthal. Optimal scaling for various Metropolis-Hastings algorithms. *Statistical Science*, 16(4):351–367, 2001.

G. O. Roberts and R. L. Tweedie. Exponential convergence of Langevin distributions and their discrete approximations. *Bernoulli*, 2(4):341–363, 1996.

G. O. Roberts and R. L. Tweedie. Bounds on regeneration times and convergence rates for Markov chains. *Stochastic Processes and Their Applications*, 80(2):211–229, 1999.

J. S. Rosenthal. Minorization conditions and convergence rates for Markov chain Monte Carlo. *Journal of the American Statistical Association*, 90(430):558–566, 1995.

J. S. Rosenthal. Simple confidence intervals for MCMC without CLTs. *Electronic Journal of Statistics*, 11:211–214, 2017.

V. Roy. Convergence diagnostics for Markov chain Monte Carlo. *Annual Review of Statistics and Its Application*, 7:387–412, 2019.

L. Song, J. Huang, A. Smola, and K. Fukumizu. Hilbert space embeddings of conditional distributions with applications to dynamical systems. In *Proceedings of the 26th International Conference on Machine Learning*, 2009.

L. F. South, T. Karvonen, C. Nemeth, M. Girolami, and C. Oates. Semi-exact control functionals from Sard’s method. *arXiv:2002.00033*, 2020.

C. Stein. A bound for the error in the normal approximation to the distribution of a sum of dependent random variables. In *Proceedings of 6th Berkeley Symposium on Mathematical Statistics and Probability*, pages 583–602. University of California Press, 1972.

M. Strocchi, M. A. Gsell, C. M. Augustin, O. Razeghi, C. H. Roney, A. J. Prassl, E. J. Vigmond, J. M. Behar, J. S. Gould, C. A. Rinaldi, M. J. Bishop, G. Plank, and S. A. Niederer. Simulating ventricular systolic motion in a four-chamber heart model with spatially varying robin boundary conditions to model the effect of the pericardium. *Journal of Biomechanics*, 101:109645, 2020.

M. A. Tanner and W. H. Wong. The calculation of posterior distributions by data augmentation. *Journal of the American statistical Association*, 82(398):528–540, 1987.

L. Tierney. Markov chains for exploring posterior distributions. *The Annals of Statistics*, 22(4):1701–1728, 1994.

D. Vats and J. M. Flegal. Lugsail lag windows and their application to MCMC. *arXiv:1809.04541*, 2018.

D. Vats and C. Knudson. Revisiting the Gelman-Rubin diagnostic. *arXiv:1812.09384*, 2018.

D. Vats, J. M. Flegal, and G. L. Jones. Multivariate output analysis for Markov chain Monte Carlo. *Biometrika*, 106(2):321–337, 2019a.

D. Vats, N. Robertson, J. M. Flegal, and G. L. Jones. Analyzing MCMC output. *arXiv:1907.11680*, 2019b.

V. Volterra. Variazioni e fluttuazioni del numero d'individui in specie animali conviventi. *Memoria della Reale Accademia Nazionale dei Lincei*, 6:31–113, 1926.

W. Xu and T. Matsuda. A Stein goodness-of-fit test for directional distributions. *arXiv:2002.06843*, 2020.

## A Proofs

This appendix contains detailed proofs for all novel theoretical results in the main text.

### A.1 Proof of Theorem 1

First we state and prove two elementary results that will be useful:

**Lemma 1.** *For all  $a, b \geq 0$  it holds that  $2a\sqrt{a^2 + b} \leq 2a^2 + b$ .*

*Proof.* Since all quantities are non-negative, we may square both sides to get an equivalent inequality  $4a^2(a^2 + b) \leq (2a^2 + b)^2$ . Expanding the brackets and cancelling terms leads to  $0 \leq b^2$ , which is guaranteed to hold.  $\square$

**Lemma 2.** *For all  $m \in \mathbb{N}$  it holds that  $\sum_{j=1}^m \frac{1}{j} \leq 1 + \log(m)$ .*

*Proof.* Since  $x \mapsto \frac{1}{x}$  is convex on  $x \in (0, \infty)$ , we have that the Riemann sum  $\sum_{j=2}^m \frac{1}{j}$  is a lower bound for the Riemann integral  $\int_1^m \frac{1}{x} dx = \log(m)$ . Thus  $\sum_{j=1}^m \frac{1}{j} = 1 + \sum_{j=2}^m \frac{1}{j} \leq 1 + \log(m)$ , as required.  $\square$

Now we present the proof of Theorem 1:

*Proof of Theorem 1.* Let  $a_m := m^2 D_{k_P}(\frac{1}{m} \sum_{j=1}^m \delta(x_{\pi(j)}))^2$ ,  $f_m := \sum_{j=1}^m k_P(x_{\pi(j)}, \cdot)$  and also let  $S^2 := \max_{i=1, \dots, n} k_P(x_i, x_i)$ , so that

$$\begin{aligned} a_m &= \sum_{j=1}^m \sum_{j'=1}^m k_P(x_{\pi(j)}, x_{\pi(j')}) = a_{m-1} + k_P(x_{\pi(m)}, x_{\pi(m)}) + 2 \sum_{j=1}^{m-1} k_P(x_{\pi(j)}, x_{\pi(m)}) \\ &\leq a_{m-1} + S^2 + 2 \min_{y \in \{x_i\}_{i=1}^n} f_{m-1}(y). \end{aligned}$$

Recall that  $\mathcal{H}(k_P)$  denotes the reproducing kernel Hilbert space of the kernel  $k_P$  and pick an element  $h_w \in \mathcal{H}(k_P)$  of the form  $h_w := \sum_{i=1}^n w_i k_P(x_i, \cdot)$ , where the weight vector  $w$  satisfies (12). From this definition it follows that  $\|h_w\|_{\mathcal{H}(k_P)} = D_{k_P}(\sum_{i=1}^n w_i \delta(x_i))$ , which is the minimal KSD attainable under the constraint (12). Now, let  $\mathcal{M}$  denote the convex hull of  $\{k_P(x_i, \cdot)\}_{i=1}^n$ , so that  $h_w \in \mathcal{M} \subset \mathcal{H}(k_P)$  and therefore

$$\min_{y \in \{x_i\}_{i=1}^n} f_{m-1}(y) = \inf_{h \in \mathcal{M}} \langle f_{m-1}, h \rangle_{\mathcal{H}(k_P)} \leq \langle f_{m-1}, h_w \rangle_{\mathcal{H}(k_P)}. \quad (19)$$

Noting that  $a_m^2 = \|f_m\|_{\mathcal{H}(k_P)}$ , we have from (19) and Cauchy-Schwarz that

$$\min_{y \in \{x_i\}_{i=1}^n} f_{m-1}(y) \leq \sqrt{a_{m-1}} \|h_w\|_{\mathcal{H}(k_P)}$$

and therefore

$$a_m \leq a_{m-1} + S^2 + 2\sqrt{a_{m-1}} \|h_w\|_{\mathcal{H}(k_P)}. \quad (20)$$

Letting

$$C_m := \frac{1}{m} (S^2 - \|h_w\|_{\mathcal{H}(k_P)}^2) \sum_{j=1}^m \frac{1}{j}, \quad (21)$$

we will establish by induction that

$$a_m \leq m^2 (\|h_w\|_{\mathcal{H}(k_P)}^2 + C_m). \quad (22)$$

This will in turn prove the result, since

$$\begin{aligned} D_{k_P} \left( \frac{1}{m} \sum_{j=1}^m \delta(x_{\pi(j)}) \right)^2 &= \frac{a_m}{m^2} \leq \|h_w\|_{\mathcal{H}(k_P)}^2 + C_m \\ &= D_{k_P} \left( \sum_{i=1}^n w_i \delta(x_i) \right)^2 + C_m \\ &\leq D_{k_P} \left( \sum_{i=1}^n w_i \delta(x_i) \right)^2 + \left( \frac{1 + \log(m)}{m} \right) S^2, \end{aligned}$$

where the upper bound on  $C_m$  follows from the fact that  $\|h_w\|_{\mathcal{H}(k_0)} \leq S$ , combined with Lemma 2.

The remainder of the proof is dedicated to establishing the induction in (22). The base case  $m = 1$  is satisfied since  $a_1 = D_{k_P}(\delta(x_{\pi(1)})) = k_P(x_{\pi(1)}, x_{\pi(1)}) \leq S^2$  and  $C_1 = S^2 - \|h_w\|_{\mathcal{H}(k_P)}^2$ , so that  $a_1 \leq \|h_w\|_{\mathcal{H}(k_P)}^2 + C_1$ . For the inductive step, we assume that (22) holds when  $m$  is replaced by  $m - 1$  and aim to derive (22). From (20) and the inductive assumption, we have that

$$\begin{aligned} a_m &\leq a_{m-1} + S^2 + 2\sqrt{a_{m-1}}\|h_w\|_{\mathcal{H}(k_P)} \\ &\leq (m-1)^2 (\|h_w\|_{\mathcal{H}(k_P)}^2 + C_{m-1}) + S^2 + 2(m-1)\sqrt{\|h_w\|_{\mathcal{H}(k_P)}^2 + C_{m-1}}\|h_w\|_{\mathcal{H}(k_P)} \\ &= m^2 (\|h_w\|_{\mathcal{H}(k_P)}^2 + C_m) + R_m \end{aligned} \quad (23)$$

where

$$\begin{aligned} R_m &:= (m-1)^2 C_{m-1} - m^2 C_m + (1-2m)\|h_w\|_{\mathcal{H}(k_P)}^2 + S^2 \\ &\quad + 2(m-1)\sqrt{\|h_w\|_{\mathcal{H}(k_P)}^2 + C_{m-1}}\|h_w\|_{\mathcal{H}(k_P)} \end{aligned}$$

The induction (22) will therefore follow from (23) if  $R_m \leq 0$ . Now,  $R_m \leq 0$  if and only if

$$2\sqrt{\|h_w\|_{\mathcal{H}(k_P)}^2 + C_{m-1}}\|h_w\|_{\mathcal{H}(k_P)} \leq \frac{m^2 C_m - (m-1)^2 C_{m-1}}{m-1} - \frac{S^2 - \|h_w\|_{\mathcal{H}(k_P)}^2}{m-1} + 2\|h_w\|_{\mathcal{H}(k_P)}^2.$$

From Lemma 1 it must hold that

$$2\sqrt{\|h_w\|_{\mathcal{H}(k_P)}^2 + C_{m-1}}\|h_w\|_{\mathcal{H}(k_P)} \leq 2\|h_w\|_{\mathcal{H}(k_P)}^2 + C_{m-1},$$

meaning it is sufficient to show that

$$2\|h_w\|_{\mathcal{H}(k_P)}^2 + C_{m-1} \leq \frac{m^2 C_m - (m-1)^2 C_{m-1}}{m-1} - \frac{S^2 - \|h_w\|_{\mathcal{H}(k_P)}^2}{m-1} + 2\|h_w\|_{\mathcal{H}(k_P)}^2. \quad (24)$$

Algebraic simplification of (24) reveals that (24) is equivalent to

$$mC_m - (m-1)C_{m-1} \leq \frac{1}{m} (S^2 - \|h_w\|_{\mathcal{H}(k_P)}^2) \quad (25)$$

and, using (21), we verify that (25) is satisfied as an equality. This completes the inductive argument.  $\square$

## A.2 Proof of Theorem 2 and Corollary 1

First we state and prove a technical lemma that will be useful:

**Lemma 3.** Let  $\mathcal{X}$  be a measurable space and let  $P$  be a probability distribution on  $\mathcal{X}$ . Let  $k_P : \mathcal{X} \times \mathcal{X} \rightarrow \mathbb{R}$  be a reproducing kernel with  $\int_{\mathcal{X}} k_P(x, \cdot) dP(x) = 0$  for all  $x \in \mathcal{X}$ . Consider a  $P$ -invariant time-homogeneous reversible Markov chain  $(X_i)_{i \in \mathbb{N}} \subset \mathcal{X}$  generated using a  $V$ -uniformly ergodic transition kernel, such that  $V(x) \geq \sqrt{k_P(x, x)}$  for all  $x \in \mathcal{X}$ , with parameters  $R \in [0, \infty)$  and  $\rho \in (0, 1)$  in (13). Then with  $C = \frac{2\rho}{1-\rho}$  we have that

$$\sum_{i=1}^n \sum_{r \in \{1, \dots, n\} \setminus \{i\}} \mathbb{E}[k_P(X_i, X_r)] \leq C \sum_{i=1}^{n-1} \mathbb{E} \left[ \sqrt{k_P(X_i, X_i)} V(X_i) \right].$$

*Proof.* First recall that given random variables  $X, Y$  taking values in  $\mathcal{X}$ , the conditional mean embedding of the distribution  $\mathbb{P}[X|Y = y]$  is the function  $\mathbb{E}[k_P(X, \cdot)|Y = y] \in \mathcal{H}(k_P)$  (Song et al., 2009). By the reproducing property we have  $\mathbb{E}[k_P(X, y)|Y = y] = \langle k_P(y, \cdot), \mathbb{E}[k_P(X, \cdot)|Y = y] \rangle_{\mathcal{H}(k_P)}$ , hence  $\mathbb{E}[k_P(X, Y)|Y] = \langle k_P(Y, \cdot), \mathbb{E}[k_P(X, \cdot)|Y] \rangle_{\mathcal{H}(k_P)}$ . Thus

$$\begin{aligned} \mathbb{E}[k_P(X, Y)|Y] &= \langle k_P(Y, \cdot), \mathbb{E}[k_P(X, \cdot)|Y] \rangle_{\mathcal{H}(k_P)} \\ &= \|k_P(Y, \cdot)\|_{\mathcal{H}(k_P)} \left\langle \frac{k_P(Y, \cdot)}{\|k_P(Y, \cdot)\|_{\mathcal{H}(k_P)}}, \mathbb{E}[k_P(X, \cdot)|Y] \right\rangle_{\mathcal{H}(k_P)} \\ &\leq \|k_P(Y, \cdot)\|_{\mathcal{H}(k_P)} \sup_{\|h\|_{\mathcal{H}(k_P)}=1} \langle h, \mathbb{E}[k_P(X, \cdot)|Y] \rangle_{\mathcal{H}(k_P)}. \end{aligned}$$

In what follows it is convenient to introduce a new random variable  $Z$ , independent from the Markov chain, such that  $Z \sim P$ . Then, since  $\mathbb{E}[k_P(Z, \cdot)] = 0$ , we have  $\mathbb{E}[h(Z)] = 0$  for any  $h \in \mathcal{H}(k_P)$ . Hence we have that

$$\mathbb{E}[k_P(X, Y)|Y] \leq \sqrt{k_P(Y, Y)} \sup_{\|h\|_{\mathcal{H}(k_P)}=1} (\langle h, \mathbb{E}[k_P(X, \cdot)|Y] \rangle - \mathbb{E}[h(Z)]).$$

Note  $|h(x)| \leq \|h\|_{\mathcal{H}(k_P)} \sqrt{k_P(x, x)}$ , so  $\|h\|_{\mathcal{H}(k_P)} = 1$  implies  $|h(x)| \leq \sqrt{k_P(x, x)}$ , thus

$$\mathbb{E}[k_P(X, Y)|Y] \leq \sqrt{k_P(Y, Y)} \sup_{|h(x)| \leq \sqrt{k_P(x, x)}} (\mathbb{E}[h(X)|Y] - \mathbb{E}[h(Z)]).$$

From  $V$ -uniform ergodicity it follows that

$$|\mathbb{E}[h(X_n)|X_0 = y] - \mathbb{E}[h(Z)]| = |P^n(y, \cdot)h - Ph| \leq RV(y)\rho^n.$$

Applying this to  $Y = X_i$ ,  $X = X_{i+r}$ , we find

$$\mathbb{E}[k_0(X_{i+r}, X_i)|X_i] \leq R\sqrt{k_0(X_i, X_i)}V(X_i)\rho^r$$

and taking the expectation on both sides yields

$$\mathbb{E}[k_P(X_{i+r}, X_i)] \leq R\mathbb{E} \left[ \sqrt{k_P(X_i, X_i)} V(X_i) \right] \rho^r. \quad (26)$$

Finally, we can use (26) to obtain that

$$\begin{aligned} \sum_{i=1}^n \sum_{r \in \{1, \dots, n\} \setminus \{i\}} \mathbb{E}[k_P(X_r, X_i)] &= 2 \sum_{i=1}^{n-1} \sum_{r=1}^{n-i} \mathbb{E}[k_P(X_{i+r}, X_i)] \\ &\leq 2R \sum_{i=1}^{n-1} \mathbb{E} \left[ \sqrt{k_P(X_i, X_i)} V(X_i) \right] \sum_{r=1}^{n-i} \rho^r. \end{aligned}$$

Thus for  $C = 2R \sum_{r=1}^{\infty} \rho^r = \frac{2\rho}{1-\rho} < \infty$ , we have that

$$\sum_{i=1}^n \sum_{r \in \{1, \dots, n\} \setminus \{i\}} \mathbb{E}[k_P(X_r, X_i)] \leq C \sum_{i=1}^{n-1} \mathbb{E} \left[ \sqrt{k_P(X_i, X_i)} V(X_i) \right]$$

as claimed.  $\square$

We can now prove the main result:

*Proof of Theorem 2.* Taking expectations of the bound in Theorem 1, we have that

$$\begin{aligned} \mathbb{E} \left[ D_{k_P} \left( \frac{1}{m} \sum_{j=1}^m \delta(X_{\pi(j)}) \right)^2 \right] &\leq \underbrace{\mathbb{E} \left[ D_{k_P} \left( \sum_{i=1}^n w_i \delta(X_i) \right)^2 \right]}_{(*)} \\ &\quad + \left( \frac{1 + \log(m)}{m} \right) \underbrace{\mathbb{E} \left[ \max_{i=1, \dots, n} k_P(X_i, X_i) \right]}_{(**)}. \end{aligned}$$

In what follows we construct bounds for  $(*)$  and  $(**)$ .

**Bounding  $(*)$ :** To bound the term  $(*)$ , note that

$$D_{k_P} \left( \sum_{i=1}^n w_i \delta(X_i) \right) \leq D_{k_P} \left( \frac{1}{n} \sum_{i=1}^n \delta(X_i) \right)$$

due to the optimality property of the weights  $w$  presented in (12). It is therefore sufficient to study the KSD of the un-weighted empirical distribution  $\frac{1}{n} \sum_{i=1}^n \delta(X_i)$ . To this end, we have that

$$\mathbb{E} \left[ D_{k_P} \left( \frac{1}{n} \sum_{i=1}^n \delta(X_i) \right)^2 \right] = \frac{1}{n^2} \sum_{i=1}^n \mathbb{E}[k_P(X_i, X_i)] + \frac{1}{n^2} \sum_{i=1}^n \sum_{r \in \{1, \dots, n\} \setminus \{i\}} \mathbb{E}[k_P(X_i, X_r)]. \quad (27)$$

To bound the first term in (27) we use Jensen's inequality:

$$\begin{aligned} \frac{1}{n^2} \sum_{i=1}^n \mathbb{E} [k_P(X_i, X_i)] &= \frac{1}{n^2} \sum_{i=1}^n \mathbb{E} \left[ \frac{1}{\gamma} \log e^{\gamma k_P(X_i, X_i)} \right] \\ &\leq \frac{1}{\gamma n^2} \sum_{i=1}^n \log (\mathbb{E} [e^{\gamma k_P(X_i, X_i)}]) \leq \frac{\log(b)}{\gamma n} \end{aligned}$$

The second term in (27) can be bounded via Lemma 3:

$$\frac{1}{n^2} \sum_{i=1}^n \sum_{r \in \{1, \dots, n\} \setminus \{i\}} \mathbb{E} [k_P(X_i, X_r)] \leq \frac{C}{n^2} \sum_{i=1}^{n-1} \mathbb{E} \left[ \sqrt{k_P(X_i, X_i)} V(X_i) \right] \leq \frac{CM(n-1)}{n^2} \leq \frac{CM}{n},$$

where  $C$  is defined in Lemma 3.

**Bounding (\*\*):** We proceed as follows:

$$\begin{aligned} \mathbb{E} \left[ \max_{i=1, \dots, n} k_P(X_i, X_i) \right] &= \mathbb{E} \left[ \frac{1}{\gamma} \log \max_{i=1, \dots, n} e^{\gamma k_P(X_i, X_i)} \right] \\ &\leq \mathbb{E} \left[ \frac{1}{\gamma} \log \sum_{i=1}^n e^{\gamma k_P(X_i, X_i)} \right] \\ &\leq \frac{1}{\gamma} \log \left( \sum_{i=1}^n \mathbb{E} [e^{\gamma k_P(X_i, X_i)}] \right) = \frac{\log(nb)}{\gamma} \end{aligned} \quad (28)$$

**Overall Bound:** Combining our bounds on (\*) and (\*\*) leads to the overall bound

$$\mathbb{E} \left[ D_{k_P} \left( \frac{1}{m} \sum_{j=1}^m \delta(X_{\pi(j)}) \right)^2 \right] \leq \frac{\log(b)}{\gamma n} + \frac{CM}{n} + \left( \frac{1 + \log(m)}{m} \right) \frac{\log(nb)}{\gamma}$$

as claimed.  $\square$

Finally we present the proof of Corollary 1:

*Proof of Corollary 1.* The proof proceeds in two stages; in the first stage we establish the result for a sub-sequence  $m = r^2$ , then in the second stage we extend it to all  $m \in \mathbb{N}$ . To simplify notation we adopt the shorthand

$$D_m := D_{k_P} \left( \frac{1}{m} \sum_{j=1}^m \delta(X_{\pi(j)}) \right)$$

in the sequel.

For the first stage, from the Markov inequality and the conclusion of Theorem 2, we have that for any  $\epsilon > 0$ ,

$$\mathbb{P}[D_m > \epsilon] \leq \frac{1}{\epsilon^2} \mathbb{E}[D_m^2] \leq \frac{c_1(m, n)}{\epsilon^2}$$

where

$$c_1(m, n) := \frac{\log(b)}{\gamma n} + \frac{CM}{n} + \left( \frac{1 + \log(m)}{m} \right) \frac{\log(nb)}{\gamma}.$$

Since  $m \leq n$  we have that

$$c_1(m, n) \leq \frac{\log(b)}{\gamma m} + \frac{CM}{m} + \left( \frac{1 + \log(m)}{m} \right) \frac{\log(nb)}{\gamma}.$$

The assumption  $\log(n) = O(m^{\beta/2})$  for some  $\beta < 1$  implies that  $\log(nb) \leq \alpha m^{\beta/2} + \log(b)$  for some constant  $\alpha \in (0, \infty)$ . Thus

$$c_1(r^2, n) \leq \frac{\log(b)}{\gamma r^2} + \frac{CM}{r^2} + \left( \frac{1 + \log(r^2)}{r^2} \right) \frac{(\alpha r^\beta + \log(b))}{\gamma}. \quad (29)$$

This shows that  $c_1(r^2, n) = O(\log(r)^2/r^{2-\beta})$ , and it follows that

$$\sum_{r=1}^{\infty} \mathbb{P}[D_{r^2} > \epsilon] \leq \frac{1}{\epsilon^2} \sum_{r=1}^{\infty} c_1(r^2, n) < \infty.$$

From the Borel-Cantelli lemma there almost surely exists  $r_1 \in \mathbb{N}$  such that  $D_{r^2} \leq \epsilon$  for all  $r \geq r_1$ . Since this argument holds for every  $\epsilon > 0$ , it follows that  $D_{r^2} \rightarrow 0$  almost surely as  $r \rightarrow \infty$ .

For the second stage we argue that, for  $r^2 \leq m < (r+1)^2$ ,

$$\begin{aligned} |D_m^2 - D_{r^2}^2| &= \frac{1}{m^2} |m^2 D_m^2 - m^2 D_{r^2}^2| \leq \frac{1}{m^2} |m^2 D_m^2 - r^4 D_{r^2}^2| + \frac{1}{m^2} |(m^2 - r^4) D_{r^2}^2| \\ &\leq \frac{1}{r^4} |m^2 D_m^2 - r^4 D_{r^2}^2| + \frac{2(r+1)}{r^2} D_{r^2}^2, \end{aligned}$$

and also that, using the reproducing property and Cauchy-Schwarz,

$$\begin{aligned} |m^2 D_m^2 - r^4 D_{r^2}^2| &= \left| \sum_{i,j=r^2+1}^m k_P(X_{\pi(i)}, X_{\pi(j)}) \right| \\ &\leq \sum_{i,j=r^2+1}^m \sqrt{k_P(X_{\pi(i)}, X_{\pi(i)})} \sqrt{k_P(X_{\pi(j)}, X_{\pi(j)})} \\ &\leq (m - r^2)^2 \max_{1 \leq i \leq n} k_P(X_i, X_i) \leq 4r^2 \max_{1 \leq i \leq n} k_P(X_i, X_i), \end{aligned}$$

so that overall

$$\begin{aligned}\mathbb{E} \left[ \max_{r^2 \leq m < (r+1)^2} |D_m^2 - D_{r^2}^2| \right] &\leq \frac{4}{r^2} \mathbb{E} \left[ \max_{1 \leq i \leq n} k(X_i, X_i) \right] + \frac{2(r+1)}{r^2} \mathbb{E} [D_{r^2}^2] \\ &\leq \frac{4}{r^2} \frac{\log(nb)}{\gamma} + \frac{2(r+1)}{r^2} c_1(r^2, n) =: c_2(r, n)\end{aligned}$$

where we have used (28) to arrive at the final bound. Using (29) and the bound  $\log(nb) \leq \alpha m^{\beta/2} + \log(b)$ , the quantity  $c_2(r, n)$  just defined satisfies

$$c_2(r, n) \leq \frac{4}{r^2} \frac{(\alpha r^{\beta/2} + \log(b))}{\gamma} + \frac{2(r+1)}{r^2} \left( \frac{\log(b)}{\gamma r^2} + \frac{CM}{r^2} + \left( \frac{1 + \log(r^2)}{r^2} \right) \frac{(\alpha r^\beta + \log(b))}{\gamma} \right),$$

which is  $O(1/r^{2-\beta/2})$ . Using the Markov inequality and the fact that  $(a+b)^2 \leq |a^2 - b^2|$ , for any  $\epsilon > 0$ ,

$$\begin{aligned}\sum_{r=1}^{\infty} \mathbb{P} \left[ \max_{r^2 \leq m < (r+1)^2} |D_m - D_{r^2}| > \epsilon \right] &\leq \frac{1}{\epsilon^2} \sum_{r=1}^{\infty} \mathbb{E} \left[ \max_{m^2 \leq m < (r+1)^2} |D_m - D_{r^2}|^2 \right] \\ &\leq \frac{1}{\epsilon^2} \sum_{r=1}^{\infty} \mathbb{E} \left[ \max_{r^2 \leq m < (r+1)^2} |D_m^2 - D_{r^2}^2| \right] \\ &\leq \frac{1}{\epsilon^2} \sum_{r=1}^{\infty} c_2(r, n) < \infty.\end{aligned}$$

From the Borel-Cantelli lemma there almost surely exists  $r_2 \in \mathbb{N}$  such that

$$\max_{r^2 \leq m < (r+1)^2} |D_m - D_{r^2}| \leq \epsilon$$

for all  $r \geq r_2$ . Since this argument holds for every  $\epsilon > 0$ , it follows that  $D_m \rightarrow D_{r^2}$  almost surely, where  $r^2 \leq m < (r+1)^2$  and  $r \rightarrow \infty$ . It therefore follows that  $D_m \rightarrow 0$  almost surely as  $m \rightarrow \infty$ .

Finally, under the assumptions of Proposition 3,  $D_m \rightarrow 0$  implies that  $\frac{1}{m} \sum_{j=1}^m \delta(X_{\pi(j)}) \Rightarrow P$ . It immediately follows that  $\frac{1}{m} \sum_{j=1}^m \delta(X_{\pi(j)}) \Rightarrow P$  almost surely, as claimed.  $\square$

## B Software

To assist with applications of **Stein Thinning** we have provided code<sup>1</sup> in both Python and MATLAB. In this section we demonstrate **Stein Thinning** in Python, but the syntax for **Stein Thinning** in MATLAB is almost identical. As an illustration of how **Stein Thinning** can be used to post-process output from **Stan**, consider the following simple **Stan** script that produces 1000 correlated samples from a bivariate Gaussian model:

---

<sup>1</sup>The Python code is available at [https://github.com/wilson-ye-chen/stein\\_thinning](https://github.com/wilson-ye-chen/stein_thinning) and the MATLAB code is available at [https://github.com/wilson-ye-chen/stein\\_thinning\\_matlab](https://github.com/wilson-ye-chen/stein_thinning_matlab).

```

from pystan import StanModel
mc = """
parameters {vector[2] x;}
model {x ~ multi_normal([0, 0], [[1, 0.8], [0.8, 1]]);}
"""
sm = StanModel(model_code=mc)
fit = sm.sampling(iter=1000)

```

The bivariate Gaussian model is used for illustration, but regardless of the complexity of the model being sampled the output of `Stan` will always be a `fit` object. The sampled points  $x_i$  and the gradients  $\nabla \log p(x_i)$  can be extracted from the returned `fit` object:

```

import numpy as np
smpl = fit['x']
grad = np.apply_along_axis(fit.grad_log_prob, 1, smpl)

```

One can then perform Stein Thinning to obtain a subset of  $m = 40$  states by running the following code:

```

from stein_thinning.thinning import thin
x, g = thin(smpl, grad, 40)

```

The `thin` function returns a pair of NumPy arrays, one containing the selected samples  $x$  and their corresponding gradients  $g$ . The default usage requires no additional user input and is based on the `sclmed` heuristic from Section 3.4, informed by the empirical analysis of Section 4. Alternatively, the user can choose to specify which heuristic to use for computing the preconditioning matrix  $\Gamma$  by setting the option string `pre` to either `'med'`, `'sclmed'`, `'smpcov'`, `'bayesian'`, or `'avehess'`. For example, the default setting corresponds to

```
x, g = thin(smpl, grad, 40, pre='sclmed')
```

The ease with which Stein Thinning can be used makes it possible to consider a wide variety of applications, including the ODE models that we considered in Section 4.

## C Experimental Protocol

Here we fill in remaining details, providing a complete description of the experiments performed in Section 4.

Recall, for the ODE models that we considered in Section 4, we required pointwise evaluation of  $\nabla \log \mathcal{L}$ . Straight-forward application of the chain rule leads to the following expression for this gradient:

$$(\nabla \log \mathcal{L})(x) = - \sum_{i=1}^N \frac{\partial u}{\partial x}(t_i) (\nabla \log \phi_i)(u(t_i)),$$

Proposal	$H$	$G$	Details
RW	0	$\epsilon I$	Step size $\epsilon$ selected following Roberts and Rosenthal (2001)
ADA-RW (Haario et al., 1999)	0	$\sqrt{\hat{\Sigma}}$	$\hat{\Sigma}$ is the sample covariance matrix of preliminary MCMC output
MALA (Roberts and Tweedie, 1996)	$\frac{\epsilon^2}{2} I$	$\epsilon I$	Step size $\epsilon$ selected following Roberts and Rosenthal (2001)
PRECOND-MALA (Girolami and Calderhead, 2011)	$\frac{\epsilon^2}{2} M^{-1}(x_{n-1})$	$\epsilon \sqrt{M^{-1}(x_{n-1})}$	$M(x) = F(x) + \Sigma_0^{-1}$ where $F(x)$ is the Fisher information matrix at $x$ and $\Sigma_0$ is the prior covariance matrix.

Table 4: Parameters  $H$  and  $G$  used in the Metropolis–Hastings proposal.

where  $(\partial u / \partial x)_{r,s} := \partial u_r / \partial x_s$  is the matrix of *sensitivities* of the solution  $u$  to the parameter  $x$  and is time-dependent. Sensitivities can be computed by augmenting the system in (17) and simultaneously solving the *forward sensitivity equations*

$$\frac{d}{dt} \left( \frac{\partial u_r}{\partial x_s} \right) = \frac{\partial f_r}{\partial x_s} + \sum_{l=1}^q \frac{\partial f_r}{\partial u_l} \frac{\partial u_l}{\partial x_s} \quad (30)$$

together with the initial condition  $(\partial u_r / \partial x_s)(0) = 0$ , which follows from the independence of  $u^0$  and  $x$ .

The experiments reported in Section 4 were based on four distinct Metropolis–Hastings MCMC methods, whose details have not yet been described. Table 4 therefore contains full details for how each of the RW, ADA-RW, MALA and PRECOND-MALA samplers were implemented.

## D Additional Results

This section collects together additional empirical results that accompany the discussion in Section 4.

### D.1 Lotka–Volterra

Additional results for the Lotka–Volterra model are as follows:

- Table 5 contains the states that were used to initialise the  $L$  Markov chains that form the basis of our experiment.
- Figure 14 contains univariate convergence diagnostics for the Lotka–Volterra model.

Chain Number	RW, MALA, PRECOND-MALA	ADA-RW
1	(0.55, 1, 0.8, 0.8)	(0.55, 1, 0.8, 0.8)
2	(1.5, 1, 0.8, 0.8)	(0.55, 1, 0.8, 1.3)
3	(1.3, 1.33, 0.5, 0.8)	(1.3, 1.33, 0.5, 0.8)
4	(0.55, 3, 3, 0.8)	(0.55, 1, 1.5, 1.5)
5	(0.55, 1, 1.5, 1.5)	(0.55, 1.3, 1, 0.8)

Table 5: Initial points  $\theta = \exp(x)$ , overdispersed with respect to the posterior, for the convergence diagnostics with  $L = 5$  chains in the Lotka-Volterra model. The parameters used to generate the data were  $\theta = (0.67, 1.33, 1, 1)$ .

## D.2 The Biology of the Hinch Model

The Hinch et al. (2004) single cell model simulates the calcium transient evoked by membrane depolarisation. The model has a mathematical representation of the extracellular space and the intracellular compartment consisting of the sarcoplasmic reticulum (SR), dyadic space and cytosol. The major sarcolemmal calcium pathways are included: the L-type Ca channel (LCC), the plasmalemmal membrane calcium ATPase (PMCA) and the sodium-calcium exchanger (NCX). Inside the cell, the model has mathematical representations for calcium release from the SR to dyadic space through ryanodine receptors (RyR) and re-sequestration of calcium from the dyadic space into the SR by the SR ATPase (SERCA). Calcium buffering is also featured for the cytosol. A schematic representation of the cell model is given in Figure 10.

Membrane depolarisation is triggered by an electrical event. This causes calcium to enter through LCCs into the dyadic space, producing a local rise in Ca concentration, sufficient to activate RyRs. This process engages a feedback, whereby Ca release from the SR causes more RyR opening events. As the released Ca diffuses into the cytosol, most of it becomes buffered, but some ions remain free and underpin the Ca transient. Recovery following Ca release is driven by SERCA, which re-sequesters Ca into the SR, and NCX and PMCA which extrude calcium across the sarcolemma. This returns the cell to its initial conditions, ready for the next electrical stimulation.

The Hinch model describes the nonlinear, time-dependent interaction of the four Ca handling transporters (LCC, PMCA, RyR and SERCA) and lumped buffering by a system of 6 ordinary differential equations with 38 parameters. The model provides a simplified four-state model describing the interaction between LCC and RyR within the dyadic space. Here, only three states are simulated due to a conservation of mass constraint. The remaining differential equations describe calcium concentration in the sarcoplasmic reticulum and the cytosol, and the calcium bound to cytosolic buffers. Of these state variables, only the concentration of free calcium in the cytosol can be observed experimentally.

To provide a rich dataset for characterising calcium dynamics in a single cardiac myocyte, we applied three experimental protocols in sequence on a single myocyte. During these protocols, we controlled membrane potential and measured membrane currents electrophysiologically and followed Ca fluorimetrically, after appropriate calibration. The calcium handling proteins were interrogated by relating currents and Ca concentration in response to

defined membrane potential manoeuvres, and in the presence of drugs to eliminate various confounding components. The first voltage protocol interrogated LCC currents at different voltages, and measured their response in terms of SR release. In the second protocol, a train of depolarisations then triggered Ca transients which provided information about SR release and their recovery provided a readout of SERCA, NCX and PMCA activities. The third protocol consistent of rapid exposure to caffeine which emptied the SR and short-circuited SERCA. This provided information about SR load, and the subsequent recovery is a readout of NCX and PMCA. Buffering was calculated from the quotient of measured Ca rise upon caffeine exposure and the amount of Ca released back-calculated from sarcolemmal current generated by NCX. The dataset contains 12998 observations of cytosolic free calcium concentration observed at a 60 Hz sampling frequency, for a duration of 3 minutes. The data in the three post-processing steps is shown in Figure 15. Full details of the experimental protocol and the data pre-processing will be reported in a separate manuscript and are available on request.

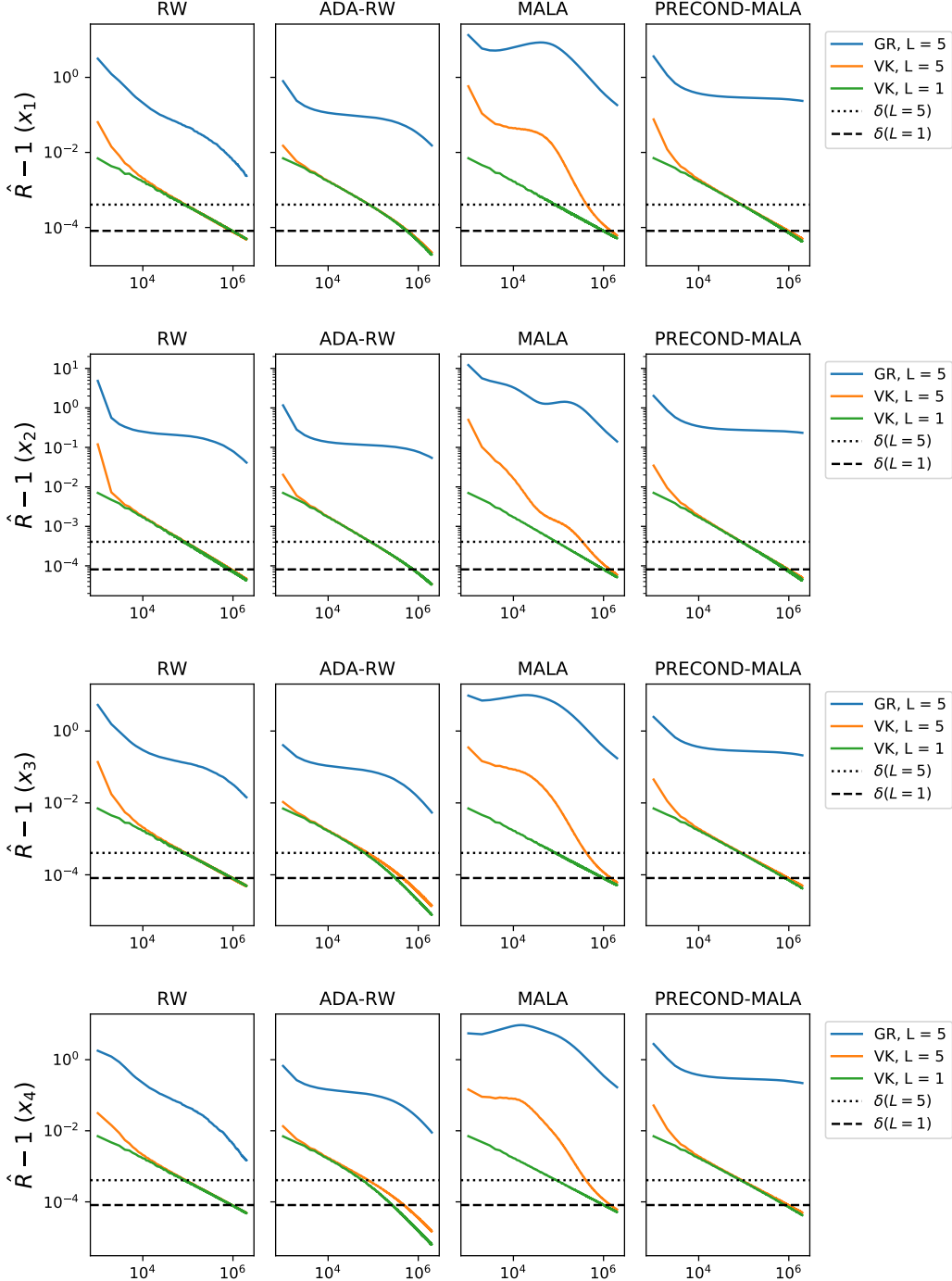


Figure 14: Univariate convergence diagnostics, for the Lotka-Volterra model, plotted against the MCMC iteration number. The blue line represents the GR diagnostic (based on  $L = 5$  chains), while the orange and green lines represent the VK diagnostic (based on  $L = 5$  and  $L = 1$  chains, respectively). The dotted ( $L = 5$ ) and dashed ( $L = 1$ ) horizontal lines correspond to the critical values  $\delta(L, \alpha, \epsilon)$ , used to determine the burn-in period; see Table 1.

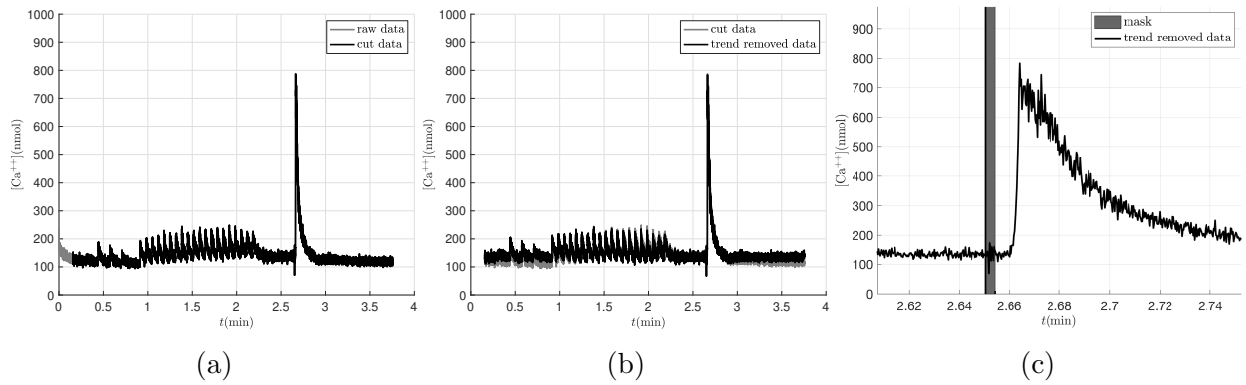


Figure 15: Calcium concentration data (in nmol) was pre-processed in three stages: (a) Extreme data were “cut”; (b) The time series was de-trended; (c) Outliers were masked.